$\Lambda\pi^-$ Production from K^- Interactions in Helium*

K. BUNNELL†
Argonne National Laboratory, Argonne, Illinois 60439
and
Northwestern University, Evanston, Illinois 60201

AND

M. DERRICK, T. FIELDS, L. G. HYMAN, AND G. KEYES‡
Argonne National Laboratory, Argonne, Illinois 60439

(Received 9 February 1970)

Results are presented of a bubble-chamber study of the interaction of negative kaons with helium yielding $\Lambda\pi^-$ or $\Sigma^0\pi^-$ in the final state. Both low-momentum kaons and kaons at rest were used. In the at-rest sample, the two-step process $K^-N \to \Sigma\pi$ followed by $\Sigma N \to \Lambda N$ accounts for $(18\pm2)\%$ of the $\Lambda\pi^-\mathrm{He}^3$ final state. Removing these Σ-Λ conversion events, on the basis of the pion kinetic energy, gives spectra that are compared with an impulse model. A good fit to the data is obtained by using a Hulthén form factor, a mixture of atomic-orbital-capture states with $(71\pm9)\%$ s state and $(29\pm9)\%$ p state. For this fit, the S-wave $\bar{K}N$ amplitude determined by Kim is used, and the P-wave amplitude is assumed to be dominated by the $Y^*(1385)$ with the coupling to $\bar{K}N$ given by $SU(3)$ symmetry. The same final state initiated by kaons in flight shows a good agreement with the predictions of the impulse model. No evidence is seen for a recently reported enhancement in the $\Lambda\pi^-$ system at 1440 MeV. The $\Lambda\pi^-pd$ final state is found to be dominated by the Σ-Λ conversion process. Stopping-K^--reaction branching ratios and cross sections are calculated and compared with impulse-model predictions. No evidence is found for a Λn bound state, and an upper limit for its production is 5×10^{-4} per stopping K^-.

I. INTRODUCTION

INTERACTIONS of negative kaons with He^4 were studied using film obtained in an exposure of a helium bubble chamber to a beam of separated K^- mesons at the Argonne zero-gradient synchrotron (ZGS).[1] Pictures were taken with stopping kaons as well as low-momentum kaons.

This paper presents results on the final states $\Lambda(\Sigma^0)\pi^-\mathrm{He}^3$, $\Lambda\pi^-pd$, and $\Lambda\pi^-ppn$. By using a bound nucleon as a target, the coupling of the $Y_1^*(1385)$ resonance to the K^-n system can be seen directly. In studies of KN interactions with free nucleons this is not possible, and an extrapolation below threshold is required. The data are compared with a recent impulse model[2] which utilizes the $\bar{K}N \to Y\pi$ scattering parameters as input and treats the He^3 as a spectator. In the at-rest analysis, the relative amounts of s and p atomic-orbital-state capture can be estimated.

The effects of final-state interactions were studied since Σ-Λ conversion effects are prominent in the observed data and complicate the study of impulsive reations.

II. EXPERIMENTAL DETAILS

A. Stopping-K^- Exposure and Analysis

The chamber[3] was built in a collaboration between physicists from Argonne and Carnegie-Mellon University and used a superconducting magnet to provide a field of 41 kG.[4] All events were found that had a single negative prong and an associated Λ with any number of positive prongs. Table I lists all reactions that could contribute to these topologies.

Two separate scans were made on the stopping-K^- film. 120 000 frames were scanned for V^0 events accompanied by one or two prongs, and 35 000 frames of the same sample were then scanned for V^0 events with one, two, or three prongs. The scanning efficiency for one- and two-prong V^0 events deduced from the two scans was $(85\pm4)\%$ for a single scan.

The $\sim$3700 candidate events were then measured and processed through the programs TVGP-GRIND.[5] Events not passing the geometry program initially were examined and remeasured. Finally, 6% of the events failed two measurements and were abandoned. From the kinematical reconstruction, there were $\sim$2400 events with an associated Λ fit and a beam momentum consistent with stopping.[6] All of these events were then

* Work supported by the U. S. Atomic Energy Commission.

† A dissertation based on this work has been submitted to Northwestern University in partial fulfillment of the requirements for the Ph.D. degree. Author now at Stanford Linear Accelerator Center, Stanford, Calif. 94305.

‡ Presently at Université Libre de Bruxelles, Belgium.

[1] For details of the beam design, chamber optics, and field calibrations, see G. Keyes, Ph.D. thesis, Northwestern University, 1969, ANL/HEP 6907 (unpublished); also, G. Keyes, M. Derrick, T. Fields, L. G. Hyman, J. G. Fetkovich, J. McKenzie, B. Riley, and I. T. Wang, Phys Rev. D 1, 66 (1970).

[2] This impulse model is described by J. Uretsky and K. Bunnell, following paper, Phys. Rev. D 1, 119 (1970).

[3] M. Derrick, T. Fields, L. Hyman, J. Loken, K. Martin, E. G. Pewitt, J. Fetkovich, and J. McKenzie, in USAEC Conference No. 660918, 1966 (unpublished).

[4] C. Laverick and G. Lobell, Rev. Sci. Instr. **36**, 825 (1965).

[5] The data reduction and other aspects of this experiment are covered more fully in K. Bunnell, Ph.D. thesis, Northwestern University, 1969, ANL/HEP 9622 (unpublished).

[6] The stopping criterion was the following: The quantity "k test" was defined as $(k \text{ test}) = (P_c - P_r)/\sigma_c$, where P_c is the beam momentum at the end of the track based on curvature information, P_r is the beam momentum at the same point based on range information, and σ_c is the error in P_c. A stopping kaon was required to have a k test less than 2.0.

kinematically fitted at both production and decay vertices, with the beam track momentum constrained to be zero. Multivertex fits were accepted if they had an over-all probability greater than 0.01. The measured beam-momentum distribution at the production vertex is shown in Fig. 1. The shape of this distribution is determined by the range-energy relation and the range straggling. We conclude from the distribution shown in Fig. 1(b) that the in-flight contamination in the at-rest events was $<6\%$.

Table II shows the assignment of all at-rest events that gave a multivertex fit. There was no difficulty in resolving the few fitting ambiguities that existed.[5] To investigate events with an associated Λ but no production fit, the $\Lambda\pi^-$ missing mass and the pion kinetic-energy spectra were plotted (Figs. 2 and 3). In Fig. 2(a), the bump at $M(\Lambda\pi^-)\sim 2.89$ GeV corresponds to Σ^0 production. For other cases as well, the events that did not give kinematic fits could be reasonably assigned to the underconstrained hypotheses in each topology.

TABLE I. Possible final states and constraint classes for the reaction $K^-\mathrm{He}^4 \to \Lambda\pi^- X$. "U" means "underconstrained."

Final state	1-prong V^0	2-prong V^0	3-prong V^0
	(A) $P_{K^-} \geqslant 0.0$		
$\Lambda\ \pi^-\ \mathrm{He}^3$	1C	4C	···
$\Lambda\ \pi^-\ pd$	U	1C	4C
$\Lambda\ \pi^-\ ppn$	U	U	1C
$\Sigma^0\ \pi^-\ \mathrm{He}^3$	U	2C	···
$\Sigma^0\ \pi^-\ pd$	U	U	2C
$\Sigma^0\ \pi^-\ ppn$	U	U	U
$\Lambda\ \pi^-\ \pi^+\ \mathrm{H}^3$	U	1C	4C
$\Lambda\ \pi^-\ \pi^+\ dn$	U	U	1C
$\Lambda\ \pi^-\ \pi^+\ ppn$	U	U	U
$\Lambda\ \pi^-\ \pi^0\ \mathrm{He}^3$	U	1C	···
$\Lambda\ \pi^-\ \pi^0\ pd$	U	U	1C
$\Lambda\ \pi^-\ \pi^0\ ppn$	U	U	U
	(B) $P_{K^-} \geqslant 290.0$ MeV/c		
$\Sigma^0\ \pi^-\ \pi^+\ \mathrm{H}^3$	U	U	2C
$\Sigma^0\ \pi^-\ \pi^+\ dn$	U	U	U
$\Sigma^0\ \pi^-\ \pi^+\ ppn$	U	U	U
$\Sigma^0\ \pi^-\ \pi^0\ \mathrm{He}^3$	U	U	U
$\Sigma^0\ \pi^-\ \pi^0\ pd$	U	U	U
$\Sigma^0\ \pi^-\ \pi^0\ ppn$	U	U	U

To correct for the loss of Λ decays at short and long distances, all plots displayed in this paper were weighted by the probability that the event would have been observed in the length interval $0.15 \leqslant L_\Lambda \leqslant 7$ cm. All events with $L_\Lambda \leqslant 0.15$ cm and $L_\Lambda \geqslant 7$ cm were removed from the sample. The lifetime obtained from the $\Lambda\pi^-\mathrm{He}^3$ events satisfying these Λ length cuts was $(2.58\pm 0.10)\times 10^{-10}$ sec, in good agreement with the world average of $(2.52\pm 0.03)\times 10^{-10}$ sec.[7]

B. In-Flight K^- Exposure and Analysis

60 000 frames were scanned for all Λ topologies originating from a K^- interaction in flight. About half of the in-flight film had a mean beam momentum at the center of the chamber of ~ 320 MeV/c, and the remainder had a beam momentum of ~ 270 MeV/c. 15 000 frames were double scanned, giving a scanning efficiency per single scan of $(89\pm 9)\%$. Figure 4 shows the measured beam momentum at the production vertex for events having a negative pion and an associated Λ. A lower beam-momentum cut was imposed at 125 MeV/c to remove possible interactions at rest.

The events were processed in essentially the same manner as the at-rest events, except that the measured momentum of the incident beam track was used in kinematic fitting. From some 1500 candidates, there were ~ 1100 events with an associated Λ and a measured beam momentum greater than 125 MeV/c. The numbers of events giving multivertex fits in the various topologies are shown in Table III.

As in the at-rest case, the events were weighted and the sample cut to correct for Λ detection inefficiencies. Figures 5 and 6 show the $\Lambda\pi^-$ missing mass and pion kinetic-energy distributions in the c.m. system for the in-flight events. The Σ^0 bump is evident in Fig. 5(a) at $M(\Lambda\pi^-)\sim 2.89$ GeV. Fitting ambiguities were easily resolved and the nonfit events were attributed to the underconstrained class of events.

TABLE II. Fitted events from stopping K^-.

Topology	Hypothesis	No. of events
One-prong V^0	$\pi^-\ \Lambda\ \mathrm{He}^3$	826
	$\pi^-\ \Sigma^0\ \mathrm{He}^3$	153[a]
Two-prong V^0	$\pi^-\ \Lambda\ \mathrm{He}^3$	615
	$\pi^-\ \Sigma^0\ \mathrm{He}^3$	12
	$\pi^-\ \Lambda\ pd$	289
Three-prong V^0	$\pi^-\ \Lambda\ pd$	212
	$\pi^-\ \Sigma^0\ pd$	3
	$\pi^-\ \Lambda\ ppn$	116

[a] Not fitted.

III. RESULTS

A. Reaction $K^-\mathrm{He}^4 \to \Lambda(\Sigma^0)\pi^-\mathrm{He}^3$ for Kaons at Rest

1. Energy Distributions

The Dalitz plot for the $\Lambda\pi^-\mathrm{He}^3$ final state is shown in Fig. 7. The impulsive nature of the interaction is

TABLE III. Fitted events from in-flight K^-.

Topology	Hypothesis	No. of events
One-prong V^0	$\pi^-\ \Lambda\ \mathrm{He}^3$	203
	$\pi^-\ \Sigma^0\ \mathrm{He}^3$	63[a]
Two-prong V^0	$\pi^-\ \Lambda\ \mathrm{He}^3$	103
	$\pi^-\ \Sigma^0\ \mathrm{He}^3$	15
	$\pi^-\ \Lambda\ pd$	148
	$\pi^-\ \pi^+\ \Lambda\ \mathrm{H}^3$	6
Three-prong V^0	$\pi^-\ \Lambda\ pd$	212
	$\pi^-\ \Lambda\ ppn$	217
	$\pi^-\ \Sigma^0\ pd$	25
	$\pi^-\ \pi^+\ \Lambda\ \mathrm{H}^3$	3
	$\pi^-\ \pi^+\ \Lambda\ dn$	3

[a] Not fitted.

[7] Particle Data Group, Rev. Mod. Phys. 41, 109 (1969).

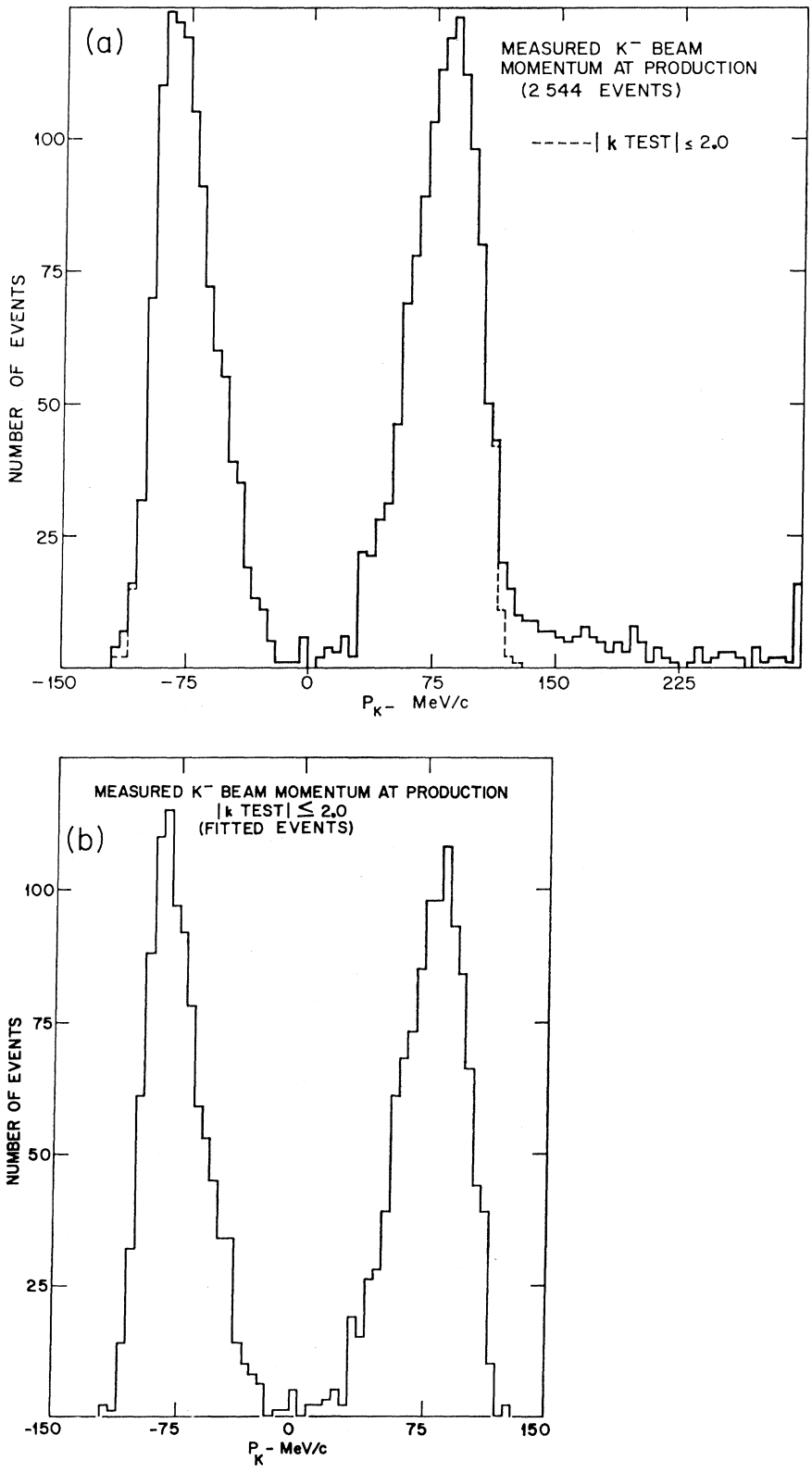

FIG. 1. Measured beam-momentum distribution at the production vertex. (a) All events with an associated Λ (solid histogram). Events with $|k \text{ test}| \leq 2.0$ (dashed histogram). (b) All events giving a production fit with the beam momentum constrained to be zero.

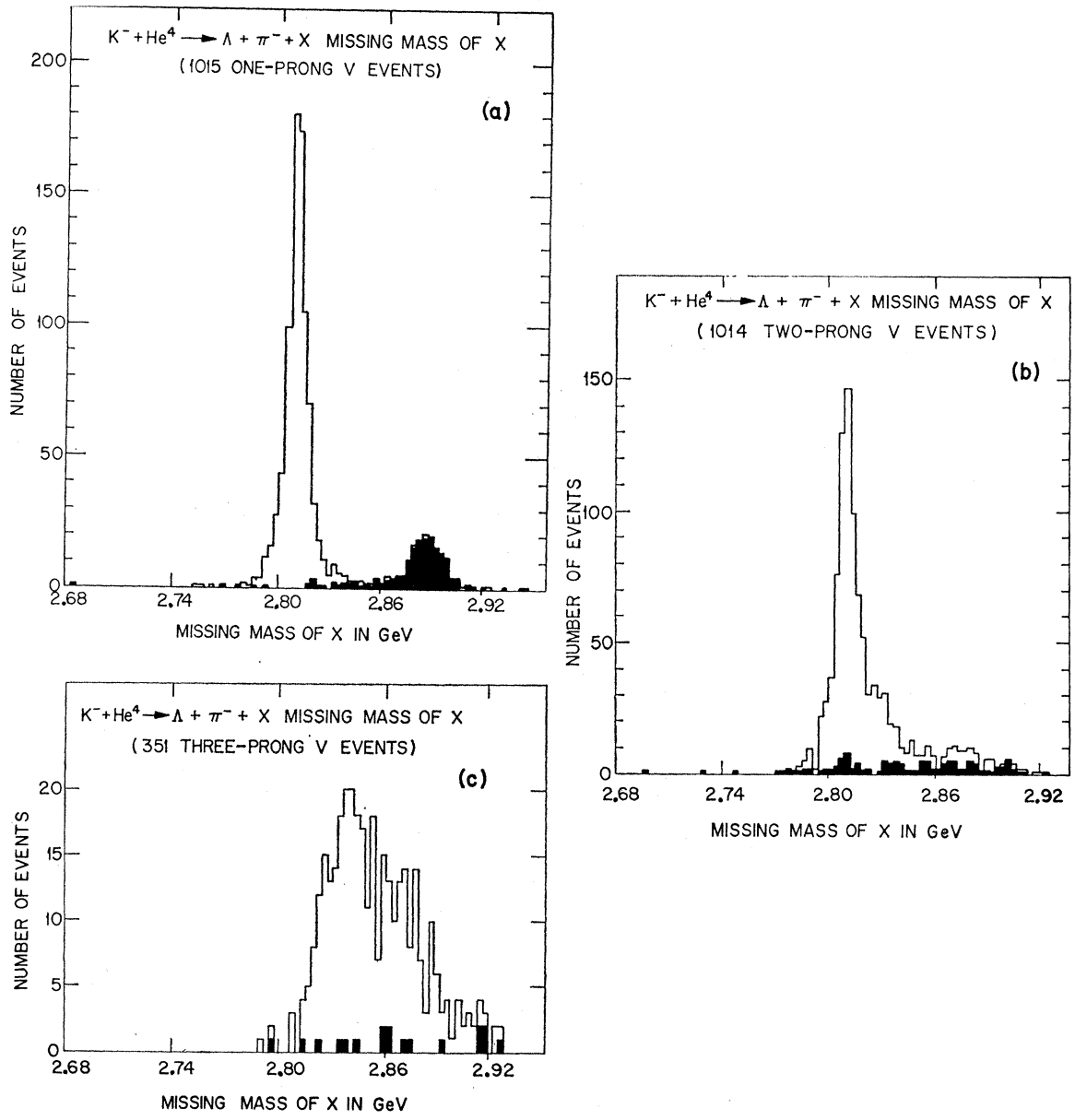

FIG. 2. Missing-mass distribution in the reaction $K^-\text{He}^4 \rightarrow \Lambda\pi^- X$ from the at-rest sample. Darkened events are those that did not give a production fit: (a) one-prong V^0 events; (b) two-prong V^0 events; (c) three-prong V^0 events.

obvious from the heavy clustering of events toward low values of He^3 energy and thus at high values of pion energy. The smearing of the pion energy distribution comes from the nucleon momentum distribution in the nucleus. There is also a noticeable clustering of events at a pion kinetic energy of about 80 MeV which we attribute to the Σ-Λ conversion process, since this pion energy corresponds to the reaction $K^-N \rightarrow \Sigma\pi$ with a free nucleon.

The projections of the Dalitz plot are also shown in Fig. 7 together with the predictions from the impulse model using parameters that Kim obtained by fitting the $\bar{K}N$ cross-section data.[8] The curves shown are for two different helium form factors, and s and p atomic-orbital-capture states.[9] All curves are normalized to the data at low He^3 kinetic energy and high pion energy where the impulse model is expected to be a reasonable approximation. Of course, common normalization is used for both projections. There are clear disagreements between theory and the experimental distributions, outside the range covered by the different form factors.

[8] J. K. Kim, Phys. Rev. Letters 19, 1074 (1967).
[9] See Ref. 2 for complete details.

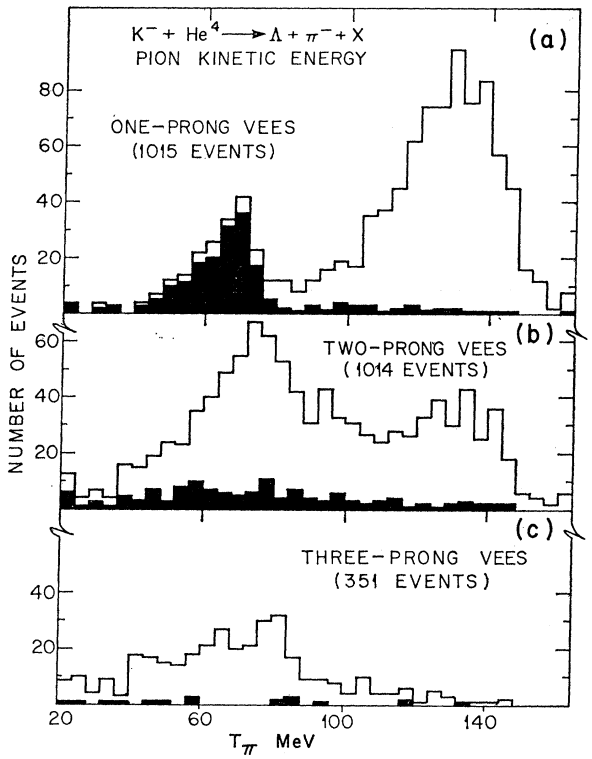

FIG. 3. Pion kinetic-energy distribution in the reaction $K^-He^4 \rightarrow \Lambda\pi^-He^3$ for the at-rest sample: (a) one-prong V^0 events; (b) two-prong V^0 events; (c) three-prong V^0 events. Darkened events are those that did not give a production fit.

In the pion kinetic-energy spectrum, there are two regions where the impulse curve does not agree with experiment.

(a) The large excess of events at pion kinetic energy below 90 MeV are in the Σ-conversion region mentioned above. As evidence that they are indeed conversion events, Fig. 21 shows the pion spectrum for the $\Lambda\pi^-pd$ events. There is considerable evidence that these breakup events originate from Σ conversion as will be discussed in Sec. III C. The pion distributions at low pion energies for the final states $\Lambda\pi^-He^3$ and $\Lambda\pi^-pd$ are very similar, indicating that they probably involve the same process.

(b) There may be evidence for some structure at a pion energy of 137 MeV in Fig. 7. This suggests a possible resonance (unbound excited state) of $_\Lambda He^4$ at an excitation of 13 MeV above zero binding energy, but our statistical accuracy is insufficient to establish the effect.

The projection on the He^3 kinetic energy shows an excess over the impulse-model prediction at higher kinetic energies. This excess could be caused by (a) Σ-Λ conversion events which give the He^3 an additional 20-MeV c.m. energy, (b) the intermediate state $Y_1^*(1385)+He^3$, which gives a He^3 kinetic energy centered at 9.1 MeV and extending from 3 to 15 MeV, and (c) other final-state interactions.

We estimate the amount of Σ-Λ conversion present to be $(18\pm2)\%$ based on the excess of events at low pion energies above the Hulthén s-state curve in Fig. 7. To simplify the subsequent analysis, most of the conversion events were eliminated from the sample by removing events with $T_\pi<90$ MeV. Using the same pion energy cut in the impulse model, and s-state capture with a Gaussian form factor, gives the comparison shown in Fig. 8. Here the theoretical curves are normalized to the events with $T_\pi>90$ MeV. One sees that the conversion cut has removed many events with a high-energy He^3 from the sample, resulting in a much better agreement with the impulse model. Note that this T_π selection should not cut seriously into the region where the $Y_1^*(1385)$ peak would be seen.

Kim's parameters are equivalent to a very small coupling between $\bar{K}N$ and the $Y_1^*(1385)$, contrary to the $SU(3)$ prediction. The $SU(3)$ curve of Fig. 8 uses Kim's S-wave parameter but uses the P_{13} amplitude predicted by $SU(3)$ symmetry with P_{11} set to zero. In the $SU(3)$ prediction, the relative phase of the S-P_{13}

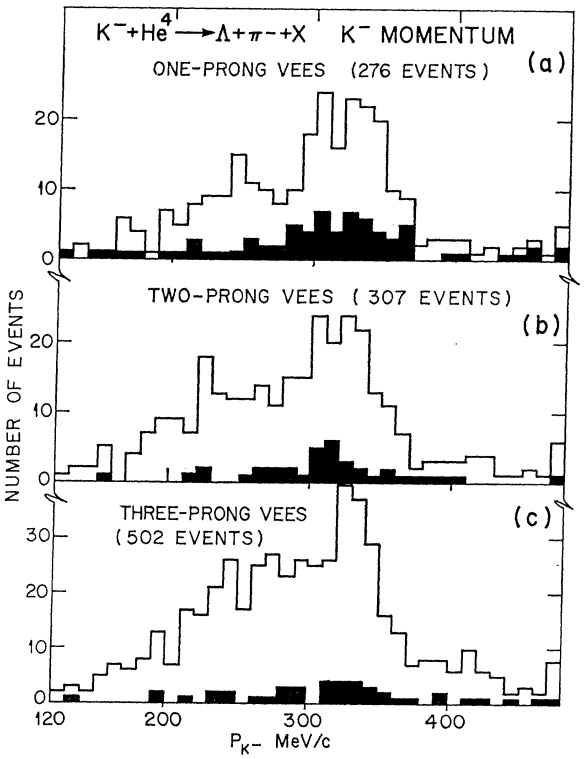

FIG. 4. Measured beam-momentum distribution for all in-flight events giving a Λ fit and having a beam momentum $\geqslant 125$ MeV/c: (a) one-prong V^0 events; (b) two-prong V^0 events; (c) three-prong V^0 events. Darkened events are those that did not give a production fit.

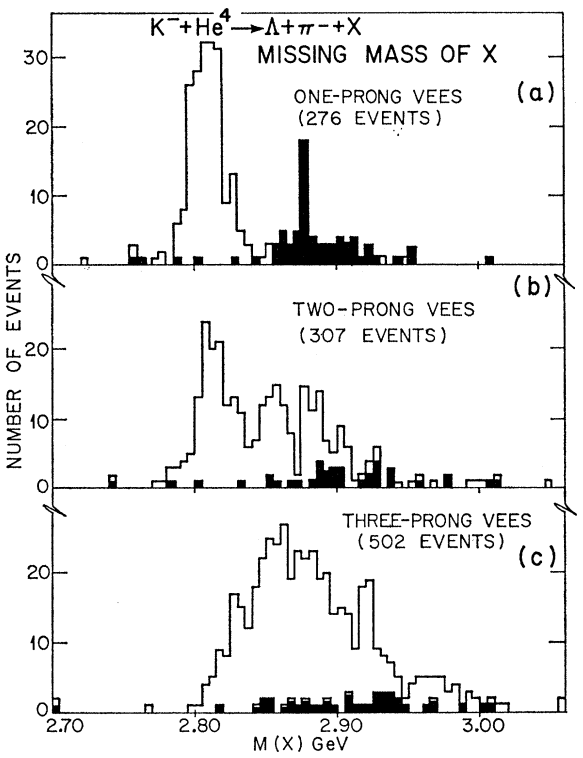

FIG. 5. Missing-mass distribution for events from in-flight sample in reaction $K^-He^4 \to \Lambda\pi^- X$ with $P_{K^-} \geqslant 125$ MeV/c: (a) one-prong V^0 events; (b) two-prong V^0 events; (c) three-prong V^0 events. Darkened events are those that did not give a production fit.

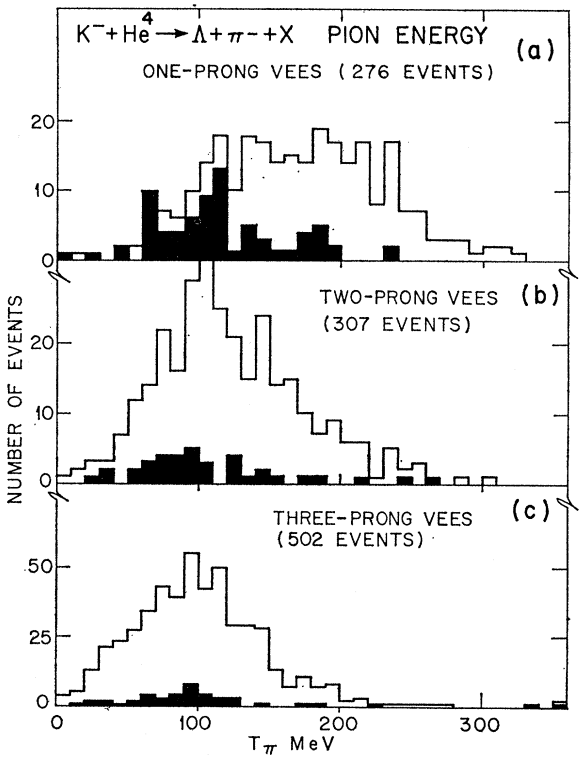

FIG. 6. Pion kinetic-energy distribution in the reation $K^-He^4 \to \Lambda\pi^- X$ from in-flight sample with $P_{K^-} \geqslant 125$ MeV/c: (a) one-prong V^0 events; (b) two-prong V^0 events; (c) three-prong V^0 events. Darkened events are those that did not give a production fit.

wave is arbitrary, and, in this case, it is chosen to be the same as in Kim's results.[10]

In the He^3 kinetic-energy spectrum of Fig. 8, the $SU(3)$ assumption gives a better fit than the Kim P-wave parameters. The pure P_{13} wave is in clear disagreement with the data, confirming Kim's conclusion that a strong S wave dominates the reaction. In particular, the strength of this S wave is qualitatively evident by the fact that a large enhancement is not predicted at 9 MeV in the He^3 kinetic-energy spectrum, even for the $SU(3)$ case.

Since the atomic-orbital state at nuclear capture is not well known,[11] the data presented here were used to estimate the fraction of captures from s- and p-atomic-orbital states (the d state was not considered). It is evident from Fig. 9(b), which shows the He^3 kinetic-energy spectrum for $T_{He^3}<6$ MeV, that the data are incompatible with pure p-state capture. In this low-energy region the results are affected very little by the form factors or matrix elements. The p-state-capture model predicts that the number of events should approach zero at $T_{He^3}=0$, which is not the experimental observation. Note that the resolution in T_{He^3} is good enough to have a negligible smearing effect on the curves of Fig. 9(b).

To estimate the fraction of s- and p-state capture, the He^3 kinetic-energy spectrum from 0 to 12 MeV was fitted with mixtures of the s and p predictions for Gaussian as well as Hulthén form factors. This was done using both the Kim and the $SU(3)$ parameters for the $\bar{K}N$ amplitudes. The results are given in Table IV. The only combination of form factor and matrix

TABLE IV. Relative fractions of s- and p-state capture.

Form factor	$\bar{K}N$ Matrix	% s state	% p state	$\chi^2(n_D=6)$
Gaussian	Kim	60± 6	40± 6	33
Gaussian	$SU(3)$	75± 8	25± 8	23
Hulthén	Kim	15±10	85±10	24
Hulthén	$SU(3)$	71± 9	29± 9	7

[10] $SU(3)$ fixes the sign of the P_{13} wave but not the sign of the S wave, since the S wave does not result from a resonance. Therefore, in a calculation based on $SU(3)$ symmetry, the relative S-P phase is a free parameter. In this paper, two values of this phase are used, one for the at-rest data (below $\bar{K}N$ threshold) and a phase differing by π for the in-flight data. The theoretical predictions for the quantities dependent on the S-P relative phase (namely, the polarization, angular distribution, and the pion kinetic-energy spectrum) are given for this particular choice. The phase could, in principle, be determined experimentally for all regions by a complete analysis of the $\bar{K}N$ data both above and below $\bar{K}N$ threshold. Lacking this analysis, our choice of phase is allowed but not compelled by existing information (see Ref. 16).

[11] G. Burleson, in *Proceedings of International Conference on Hypernuclear Physics*, edited by A. R. Bodmer and L. G. Hyman (ANL, Argonne, Ill., 1969), p. 639.

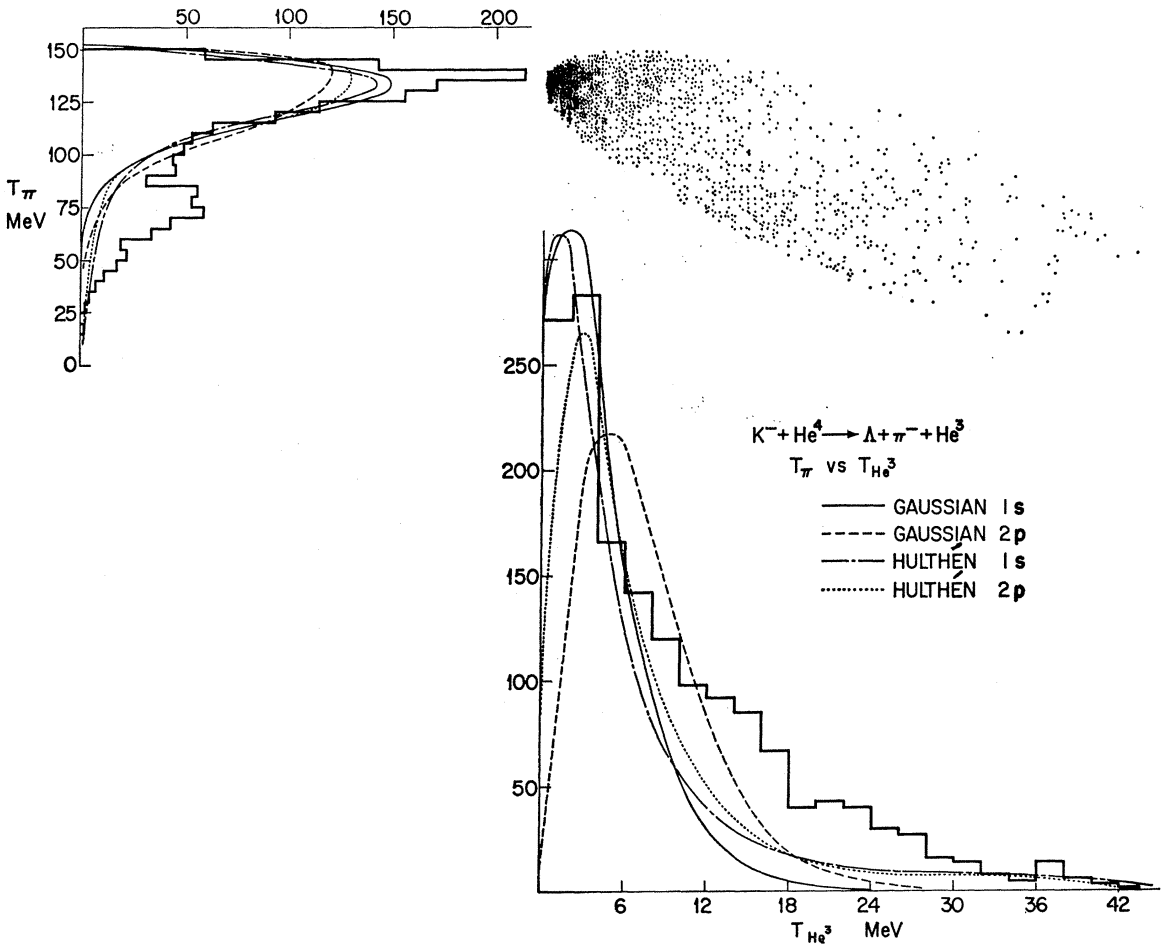

FIG. 7. Dalitz plot and projections for all events fitting $\Lambda\pi^-He^3$ at rest. The curves shown on the projections are calculated using the impulse model with Kim's parameters.

element that gives a reasonable fit ($\chi^2=7$ for 6 degrees of freedom) is a Hulthén form factor using an $SU(3)$ P_{13} $\bar{K}N$ amplitude. It should be pointed out that variations in the Gaussian size parameter, within the errors of the electron scattering data,[12] do not change the predictions appreciably. The actual curves for the fits obtained using the $SU(3)$ P_{13} wave and Kim's S wave are shown in Fig. 9(a).

There is a question whether off-mass-shell Σ-conversion events that may have remained in the sample after the pion energy cut could confuse the conclusion. This effect has been treated by Sawicki in two different calculations[13] of the Σ-conversion process in this reaction, but with inconclusive results. There are also other possible effects which could influence the conclusions. For example, capture from d states has not been included, and a possible Λ-He^3 final-state interaction has not been included. Double-scattering effects are not expected to be large.[14]

If we neglect these complications, the present results definitely favor a solution using a Hulthén form factor with 70% s-state and 30% p-state capture and $SU(3)$ $\bar{K}NY_1^*$ coupling.

2. Angular Distributions

Figure 10 shows a scatter plot of the $K^-n \rightarrow \Lambda\pi^-$ scattering angle versus the He^3 momentum. For low

[12] R. Hofstadter, Rev. Mod. Phys. **28**, 214 (1956); R. F. Frosch, T. S. McCarthy, R. E. Rand, and M. R. Yearian, Phys. Rev. **160**, 874 (1967).

[13] In the first calculation using an effective-range approximation, it was predicted that there would be essentially no contribution from the Σ conversion process in the region $T_{He^3}<12$ MeV [P. Said and J. Sawicki, Phys. Rev. **139**, B991 (1965)]. This method of calculation was identical to that used in deuterium and was based on the formalism of coupled-channel distorted waves. In a later calculation, a second-order Feynman diagram was used to consider the intermediate states [J. Sawicki, Nucl. Phys. **B1**, 183 (1967)]. In this calculation, a large amount of off-shell Σ production ($\sim$40%) was predicted and a contribution from Σ conversion in the He^3 kinetic-energy distribution for values $T_{He^3}<2$ MeV. In both calculations, the crudeness of the approximation and the uncertainties in the predictions were emphasized. There is no experimental evidence for an excess of events above the impulse calculations for $2\leqslant T_{He^3}\leqslant 12$ MeV, although there is possible evidence for some off-mass-shell Σ-conversion events for regions of He^3 kinetic energy $\gtrsim 12$ MeV.

[14] J. Sawicki, Nuovo Cimento **40**, 678 (1965).

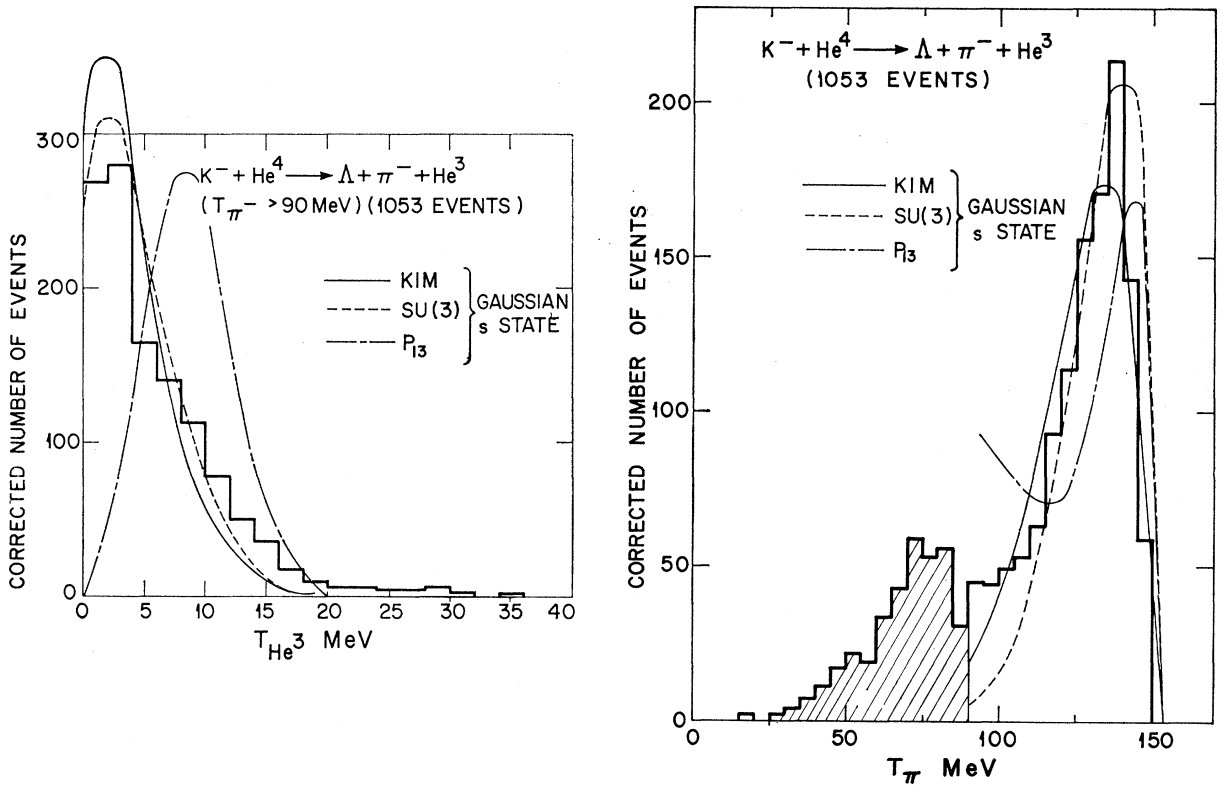

FIG. 8. He^3 and π^- kinetic-energy distribution in reaction $K^-He^4 \rightarrow \Lambda\pi^-He^3$ at rest. The He^3 spectrum is plotted for $T_{\pi^-} \geqslant 90$ MeV. Theoretical curves are (a) Gaussian form factor and s-state capture with Kim's parameters, (b) an $SU(3)$ prediction found by replacing Kim's P waves by an $SU(3)$ resonant amplitude, and (c) pure P_{13} wave. All theoretical curves are normalized to the experimental area.

values of He^3 momentum, there is a backward peaking of the Λ. For a He^3 momentum above about 250 MeV/c, the angular distribution reverses and the Λ tends to move antiparallel to the He^3 direction. These events at high He^3 momentum correspond to low-energy pions which seem to originate primarily from the Σ-Λ conversion process. Figure 11 shows the angular distribution for the two regions above and below a He^3 momentum of 250 MeV/c ($T_{He^3} = 11$ MeV).

Figure 12 shows the K^-n scattering angle for three regions of He^3 kinetic energy together with predictions from the impulse model using s-atomic-orbital-state capture and both Kim and $SU(3)$ parameters. It is seen that both theoretical curves predict some asymmetry. The experimental angular distribution, also asymmetric, might be influenced by a final-state Λ-He^3 interaction, particularly for $T_{He^3} < 8$ MeV.

3. Polarization

The values of Λ polarization as a function of He^3 energy are seen in Fig. 13 to be consistent with zero. The polarization predictions of the Kim and $SU(3)$ models are also shown and agree reasonably well with the data. The $SU(3)$ calculation is expected to be valid in the region of the $Y_1^*(3 < T_{He^3} < 15$ MeV), but not very far beyond it; hence the curve is not predicted for large He^3 energies. The polarization predicted for the $SU(3)$ model is dependent on the relative phase of the S and P waves, which is arbitrarily chosen as previously mentioned.[10]

4. Σ^0 Events

Figure 14 shows the pion spectrum for the $\Sigma^0\pi^-He^3$ events, together with the results of an impulse calculation. The criteria for identifying a $\Sigma^0\pi^-He^3$ event were either a multivertex fit or, for the one-prong V^0 events, a missing baryon mass of 2.884 ± 0.027 GeV. As can be seen from the figure, the fit to the impulse model is quite good. There is, of course, a small background as is indicated by the presence of an event outside the kinematic limit. This impulse prediction for $\Sigma^0\pi^-He^3$ does not change appreciably if $SU(3)$ P-wave predictions are used instead of Kim's P-wave parameters.

5. Comparison with Other Results

The previous experimental results[15] on the reaction $K^-He^4 \rightarrow \Lambda\pi^-He^3$ at rest had been interpreted as showing copious amounts of $Y_1^*(1385)$ being produced.

[15] J. Auman, M. M. Block, R. Gessaroli, J. Kopelman, S. Ratti, L. Grimellini, T. Kikuchi, L. Lendinara, L. Monari, and E. Harth, in *Proceedings of the 1962 International Conference on High-Energy Physics at CERN*, edited by J. Prentki (*CERN*, Geneva, 1962), p. 330.

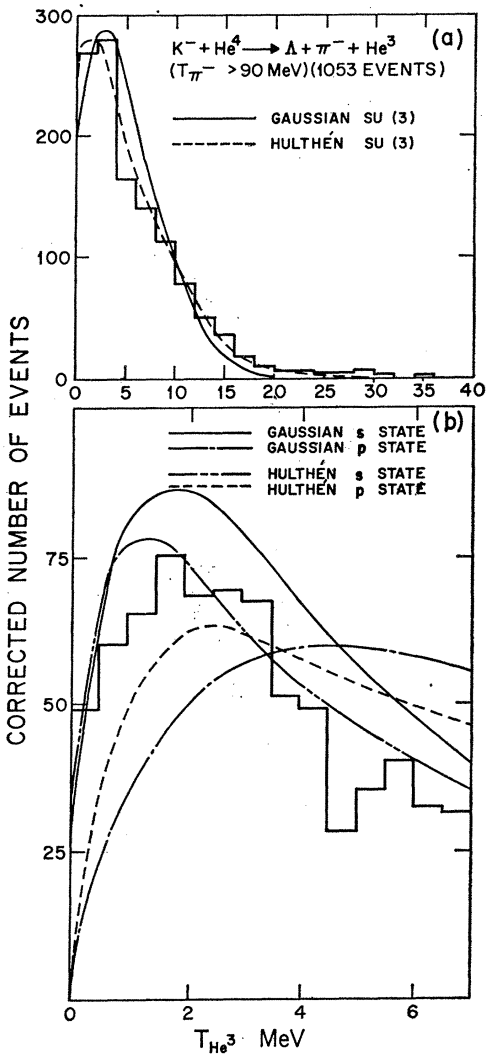

FIG. 9. (a) He^3 kinetic-energy distribution as in Fig. 8 with theoretical curves for the best fits obtained by using mixtures of s- and p-state capture with the $SU(3)$ predictions for the P_{13} wave. The Gaussian curve has 75% s-state and 25% p-state capture, whereas the Hulthén curve has 71% s-state and 29% p-state capture. (b) The low-energy part of the He^3 kinetic-energy spectrum compared to the predictions of pure s- and p-state capture for Hulthén and Gaussian wave functions. The curves are normalized to the total experimental area of the T_{He^3} spectrum shown in (a).

There are some small differences in the results reported here and those previously published, but the two sets of data are generally compatible.

The chief difference lies in the interpretation of the events at high He^3 energy ($T_{He^3}>15$ MeV) and the bump in the pion energy spectrum at about 75 MeV. In the previous experiment, these events were attributed to the production of the $Y_1^*(1385)$ in the $\Lambda\pi^-$ final state. The present analysis shows rather clearly that these events originate from the internal conversion of a Σ. From the impulse model used here, it is evident that even a pure Y_1^* amplitude could not account for

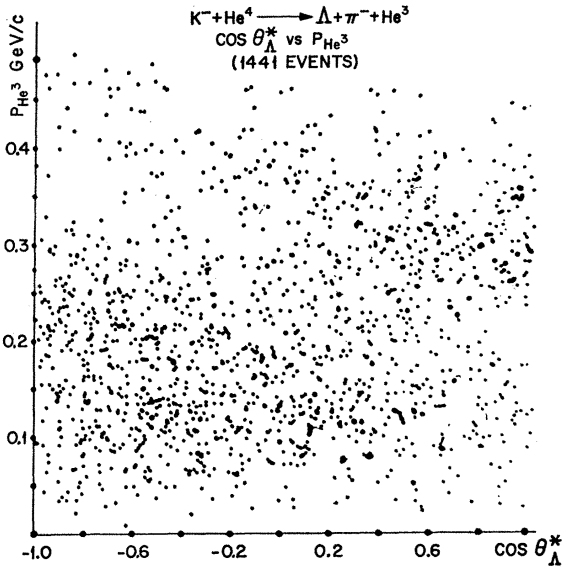

FIG. 10. Scatter plot of $\cos\theta_\Lambda^*$ versus He^3 momentum for at-rest events fitting $\Lambda\pi^-$ He^3. θ_Λ^* is the angle between the Λ and the direction of the $(\Lambda\pi)$ system measured in the $(\Lambda\pi)$ system.

the events with a He^3 kinetic energy above 20 MeV. Thus we concur with Said and Sawicki,[13] who come to similar conclusions from their analysis of the data of Auman *et al.*[15]

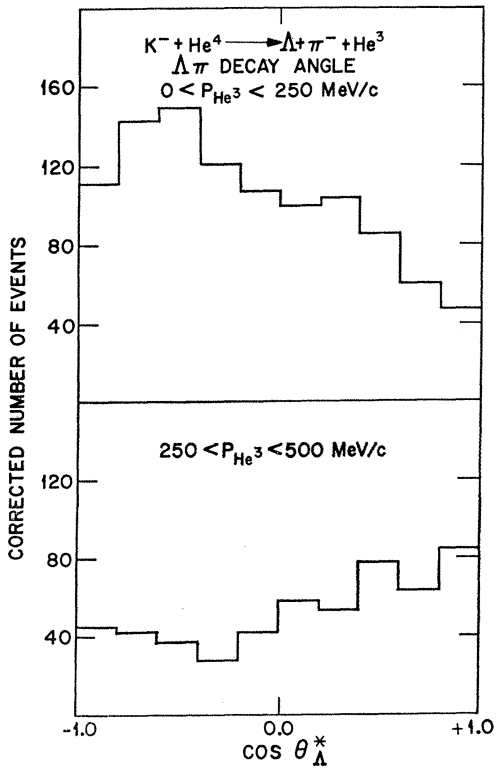

FIG. 11. Projection of Fig. 10 for two regions of He^3 momentum: (a) $0\leqslant P_{He^3}\leqslant 250$ MeV/c; (b) $250<P_{He^3}\leqslant 500$ MeV/c.

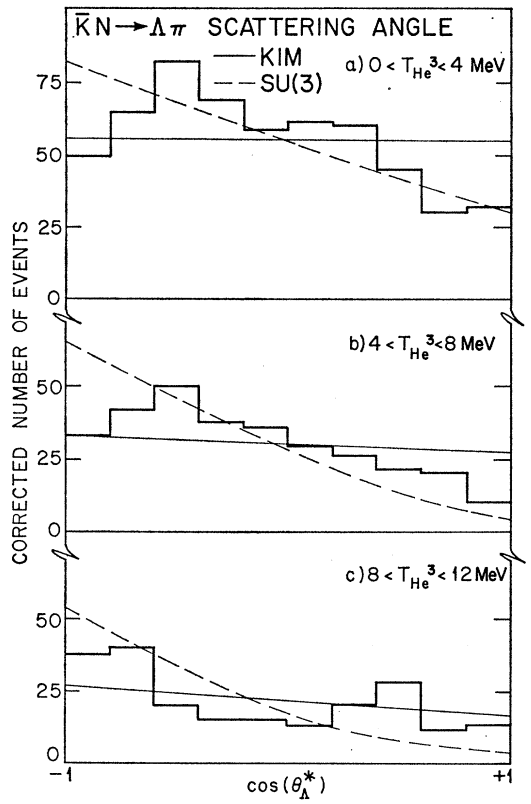

FIG. 12. Scattering-angle distribution for $K^-He^4 \rightarrow \Lambda\pi^-He^3$ at rest for three He^3 kinetic-energy regions: (a) 0–4 MeV, (b) 4–8 MeV, (c) 8–12 MeV, compared to the prediction using the Kim parameters and $SU(3)$.

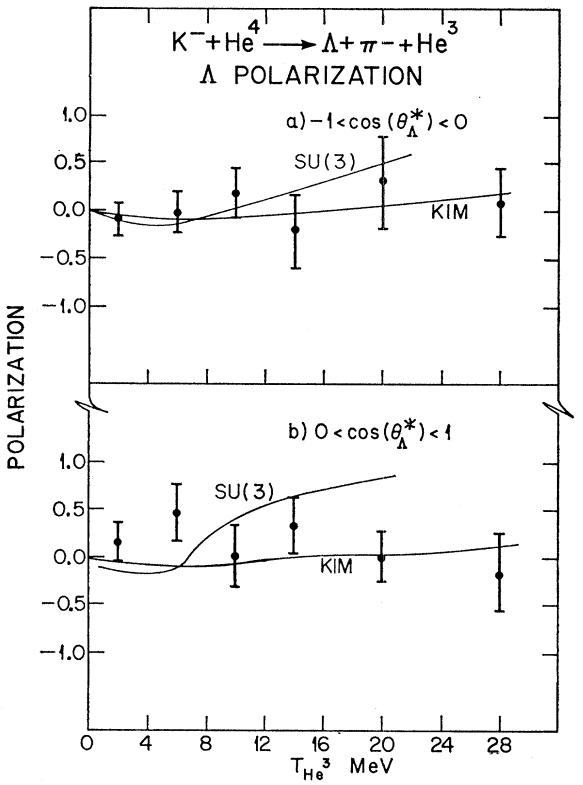

FIG. 13. Polarization of Λ as a function of He^3 kinetic energy for the final-state $\Lambda\pi^-He^3$ produced by K^- at rest. The plane is defined as $\mathbf{P}_K^* \times \mathbf{P}_\pi^*$. The theoretical curves give the Kim and $SU(3)$ predictions.

B. Reaction $K^-He^4 \rightarrow \Lambda(\Sigma)\pi^-He^3$ for Kaons in Flight

To make comparisons of quantities for the reaction $K^-He^4 \rightarrow \Lambda\pi^-He^3$ as a function of beam momentum, the data were divided into two regions, 160–280 and 280–370 MeV/c. This division gave approximately equal numbers of events in the two samples. The fact that the He^3 acts as a spectator is seen in the laboratory angular distributions of Fig. 15. The distribution is isotropic except for events where the He^3 track lies along the kaon track and so gives a scanning loss.

All spectra from the in-flight data, unless otherwise indicated, are shown in the K^-He^4 c.m. system. The pion kinetic energy is shown in Fig. 16 together with an impulse-model prediction using a Gaussian form factor and Kim's parameters, normalized to equal areas. The curves are averaged over the experimental distribution of beam momenta. The region of pion energy for Σ-conversion events is 60–140 MeV in Fig. 16(a) and 80–160 MeV in Fig. 16(b). It seems that there is some excess of events towards lower pion energies for the lower beam momentum, but the beam energy spread makes it difficult to estimate the amount of Σ-Λ conversion. The events at the higher momenta do not show any evidence for an excess of lower-energy pions, indicating that the Σ conversion process decreases in importance as the beam momentum increases.

Figure 17 shows the $\Lambda\pi^-$ invariant-mass distributions for the two intervals of kaon momentum compared to the calculations[16] using different form factors. All the curves fit the data reasonably well, although there are some small differences. In particular, at low values of $\Lambda\pi^-$ mass, the Hulthén form factor predicts more events than the Gaussian, in agreement with experiment. The $\Lambda\pi^-pd$ events shown in Fig. 32 suggest some small amount of Σ-Λ conversion, in agreement with the conclusions from the pion spectrum. For the Hulthén curves, there is no experimental excess of events in this region.

There is seen to be very little difference between the $SU(3)$ and Kim predictions, particularly for the Gauss-

[16] The replacement of the P_{13} amplitude in Kim's phase shifts by an $SU(3)$ Y_1^* amplitude may not be reasonable far from the resonance. Kim's analysis required P waves to fit the nonisotropic angular distributions observed by Kadyk [Y. Oren and J. A. Kadyk, in *Lectures in Theoretical Physics*, edited by W. B. Britten and A. O. Barut (Gordon and Breach, New York, 1967), Vol. 9B, p. 155]. In Kim's solution the P_{11} wave was dominant over the P_{13} wave. In the present analysis, in order to maintain the agreement with Kadyk's data using the $SU(3)$ P_{13} wave with $P_{11}=0$, the P_{13} S-wave relative phase is chosen to differ by π from that used in the at-rest analysis.

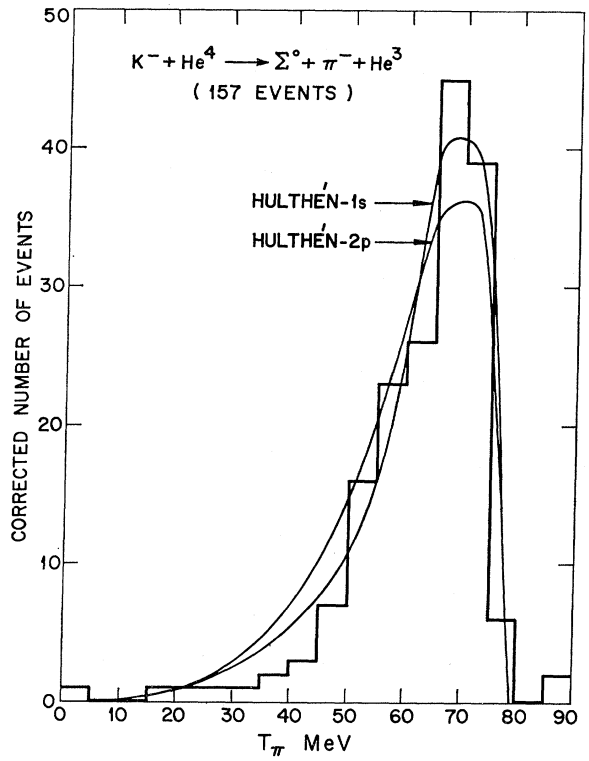

FIG. 14. Pion kinetic-energy distribution for the final-state $\Sigma^0\pi^-He^3$ produced by K^- at rest. The normalized impulse curves are calculated with the Kim matrix elements.

ian form factor. With the present statistics, all of the impulse curves fit the data equally well. Therefore, the present analysis of the $\Lambda\pi^-$ spectrum for the in-flight events does not permit a reliable determination of the form factor, the amount of Σ conversion present, or the $\bar{K}NY_1^*$ coupling.

The ΛHe^3 invariant-mass distribution is shown in Fig. 18. Unlike the at-rest events, there is no evidence for a ΛHe^3 final-state interaction 13 MeV above the ground state, but the statistics here are quite inadequate. Kim's parameters and $SU(3)$ both provide a good fit to the ΛHe^3 invariant mass. The bulk of the events are away from the region of the Y_1^* resonance and hence the $SU(3)$ curve mainly shows the high-energy tail of the resonance.

The distribution of decay angle for the $\Lambda\pi^-$ system is shown in Fig. 19. Here again the Kim amplitude and the $SU(3)$ amplitude are reasonably successful in fitting the data. Note that even for $SU(3)$, the dominant term is proportional to $\cos\theta$, indicating that neither the S nor the P wave is dominating. Kim's P-wave parametrization gives good agreement to the experimental angular distribution; this distribution is fitted less well using the $SU(3)$ coupling of $\bar{K}N$ to Y_1^*.

Table V gives the experimental results together with the theoretical predictions for Λ polarization. It is apparent that neither of the theoretical estimates is in strong disagreement, although $SU(3)$ is preferred.

As has been discussed, there is evidence for $\Sigma^0\pi^-He^3$ production, both from two-prong V^0 fitted events and from a missing-mass plot. Combining the 15 fitted events and 63 one-prong V^0 events with a missing mass between 2.82 and 2.93 GeV gives the pion spectrum shown in Fig. 20. Also shown is a beam-averaged

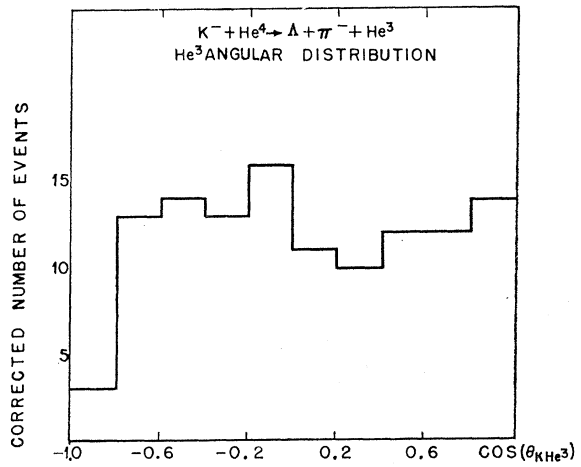

FIG. 15. Cosine of the lab angle between the observed He^3 and the K^- for in-flight $\Lambda\pi^-He^3$ events. A loss of events is seen when the beam track overlaps the He^3 stub.

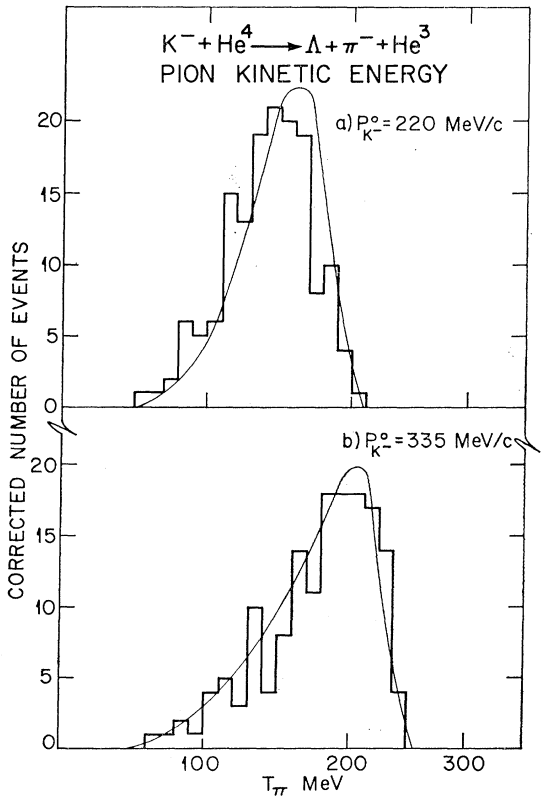

FIG. 16. Pion kinetic-energy spectra in the over-all c.m. system for the final-state $\Lambda\pi^-He^3$: (a) $160 \leqslant P_{K^-} \leqslant 280$ MeV/c; (b) $280 < P_{K^-} \leqslant 370$ MeV/c. Also shown is a normalized impulse prediction using a Gaussian form factor and Kim's matrix elements.

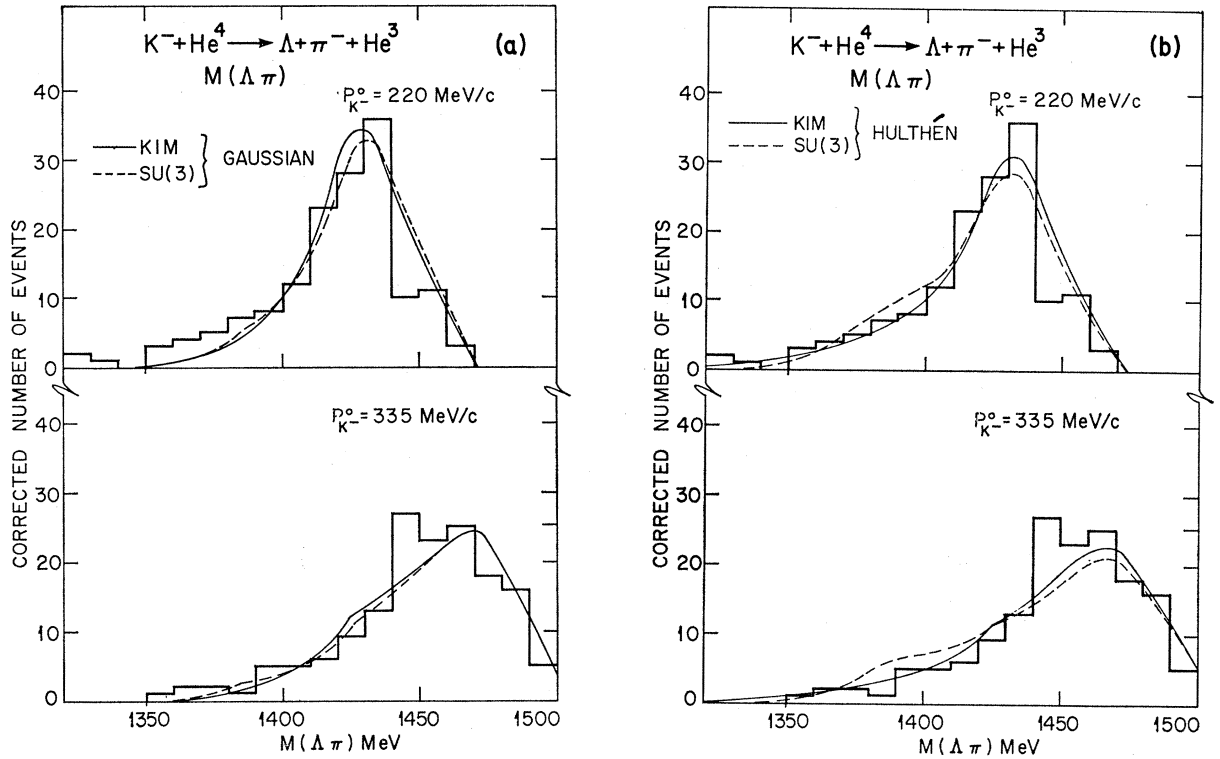

FIG. 17. $\Lambda\pi^-$ invariant-mass distributions for the final-state $\Lambda\pi^-$He^3 produced by K^- in flight. The impulse predictions are shown with the Kim and $SU(3)$ parameters for (a) Gaussian form factors and (b) Hulthén form factor.

impulse-model prediction using Kim's parameters and a Gaussian form factor. The fit seems reasonable in view of the limited statistics.

Cline *et al.*[17] have reported evidence for an enhancement at 1400 MeV in the $\Lambda\pi^-$ system from an analysis of the reaction $K^-d \rightarrow \Lambda\pi^-p$ at 400 MeV/c. The in-flight data for the reaction K^-He$^4 \rightarrow \Lambda\pi^-$He^3 can also be used to look for this enhancement. From the $\Lambda\pi^-$ invariant-mass plot shown in Fig. 17, there does not appear to be an enhancement in the region of 1440 MeV. Alexander *et al.*,[18] in analyzing the results of Cline *et al.*, deduced that the peak at 1440 MeV was likely to be consequence of the double-scattering process $K^-d \rightarrow K^-p(n_s)$ followed by $K^-n_s \rightarrow \Lambda\pi^-$. In helium, these second scattering processes are more complicated and far more difficult to calculate. The fact that no enhancement is seen at 1440 MeV in the data presented here, however, is evidence that the enhancement previously observed at 1440 MeV was not due to a $\Lambda\pi^-$

TABLE V. Λ polarization.

Beam momentum (MeV/c)	Polarization Expt.	Kim	$SU(3)$
160–280	+0.06±0.24	−0.29	+0.23
280–370	+0.08±0.24	−0.49	+0.16

[17] D. Cline, R. Laumann, and J. Mapp, Phys. Rev. Letters **21**, 1372 (1968).

[18] G. Alexander, B. H. Hall, N. Jew, G. Kalmus, and A. Kernan, Phys. Rev. Letters **22**, 483 (1969).

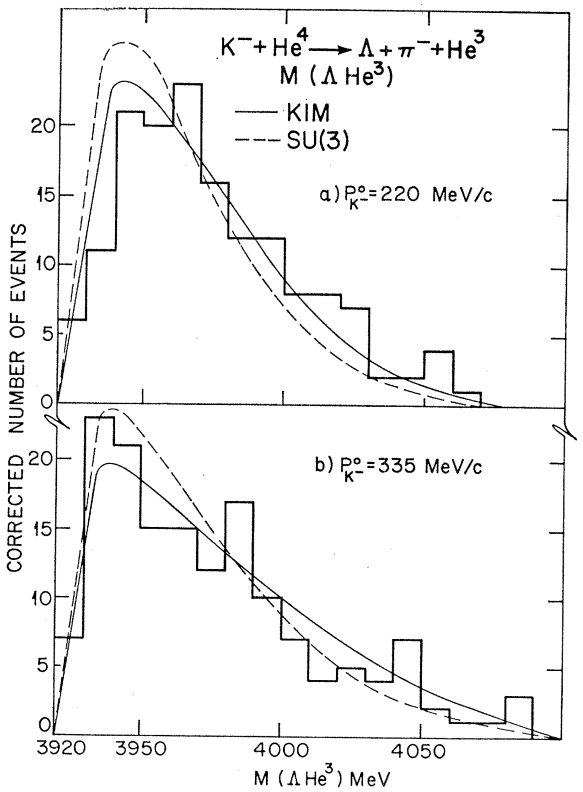

FIG. 18. Λ-He^3 invariant-mass distributions for the final-state $\Lambda\pi^-$He^3 produced by K^- compared to the impulse predictions using a Gaussian form factor.

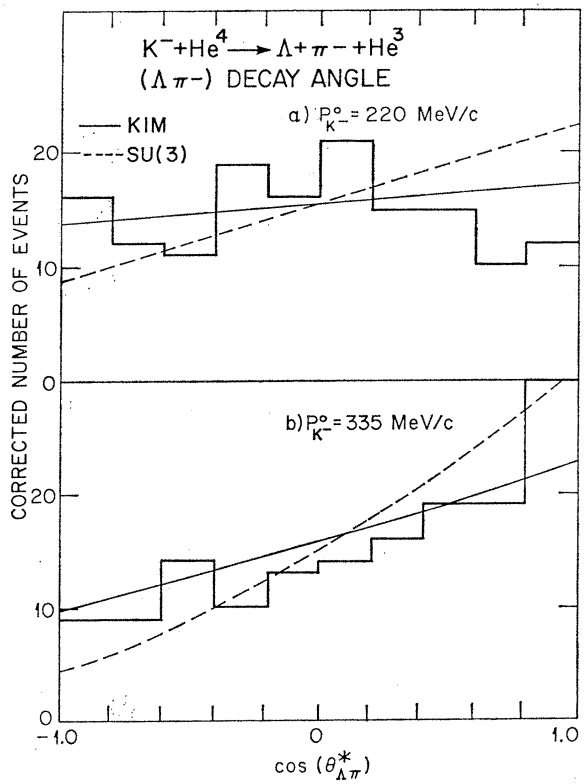

FIG. 19. $\Lambda\pi^-$ decay angle compared to predictions using a Gaussian form factor. The decay angle is defined as $\mathbf{P}_\pi^* \times \mathbf{P}_{(\Lambda\pi)}^*$ and so differs by π from the scattering angle shown in Fig. 12.

resonance, in agreement with the conclusions of Alexander *et al.*

C. Reactions $K^-He^4 \rightarrow \Lambda\pi^- pd$ and $K^-He^4 \rightarrow \Lambda\pi^- ppn$ for Kaons at Rest

Figure 21 shows a plot of the pion kinetic-energy distribution for the events fitting the $\Lambda\pi^- pd$ hypothesis. The peak in the pion kinetic-energy plot around 80

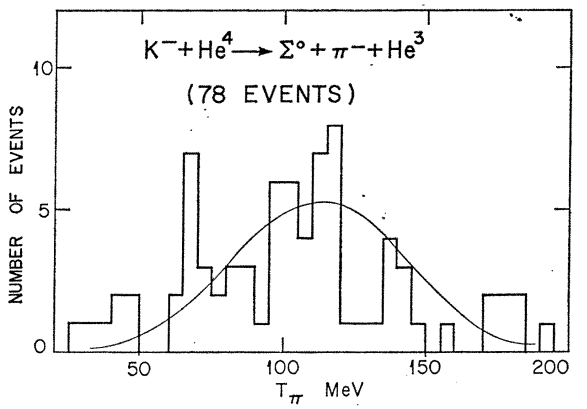

FIG. 20. Pion kinetic-energy distribution in the K^-He^4 c.m. system for in-flight $\Sigma^0\pi^-He^3$ events ($P_{K^-} \geqslant 125$ MeV/c). The curve is the prediction of the impulse model using the Kim parameters.

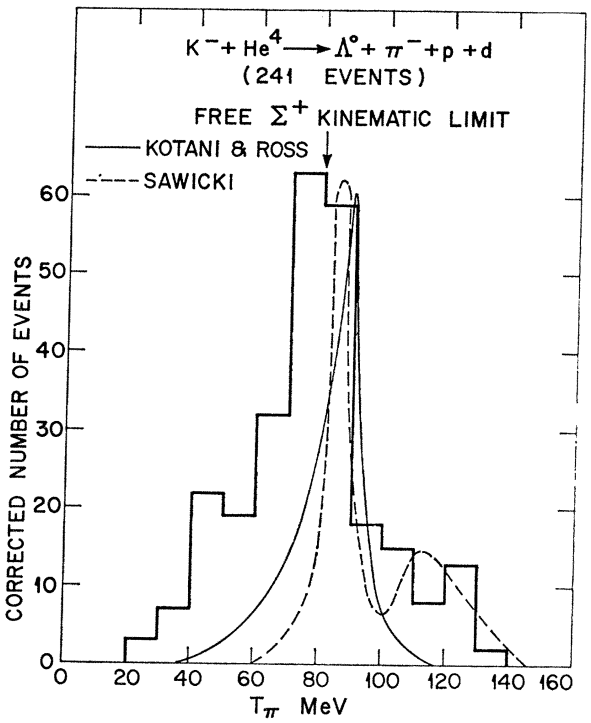

FIG. 21. Pion kinetic-energy distribution for events at rest fitting $\Lambda\pi^- pd$. The two theoretical predictions for the pion spectrum from Σ-Λ conversion are (1) for the final-state $\Lambda\pi^-He^3$ from Sawicki (dashed curve) and (2) for the reaction $K^-d \rightarrow \Lambda\pi^- p$ from Kotani and Ross (solid curve).

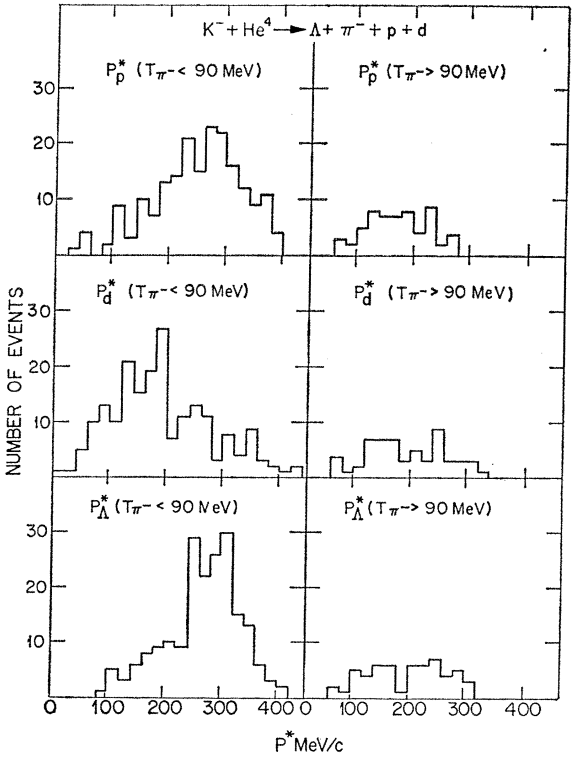

FIG. 22. Proton, Λ, and deuteron momentum spectra measured in the Λpd c.m. frame for all at-rest events fitting $\Lambda\pi^- pd$ for (a) $T_\pi \leqslant 90$ MeV and (b) $T_\pi > 90$ MeV.

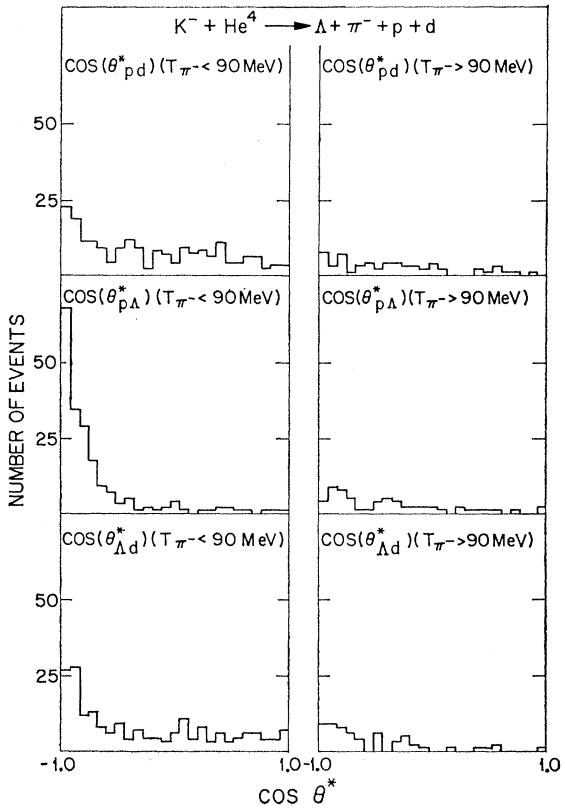

FIG. 23. Angles between proton, Λ, and deuteron for all at-rest events fitting $\Lambda\pi^- pd$ in the Λpd c.m. frame for (a) $T_\pi \leqslant 90$ MeV and (b) $T_\pi > 90$ MeV.

MeV is evidence for Σ-Λ conversion, since for the reaction $K^-\text{He}^4 \rightarrow \Sigma^+\pi^-\text{H}^3$ the maximum pion kinetic energy is 80 MeV.

A theoretical prediction of the pion distribution from Σ-Λ conversion comes from Sawicki[13] for the reaction $K^-\text{He}^4 \rightarrow \Lambda\pi^-\text{He}^3$. Calculations have also been made

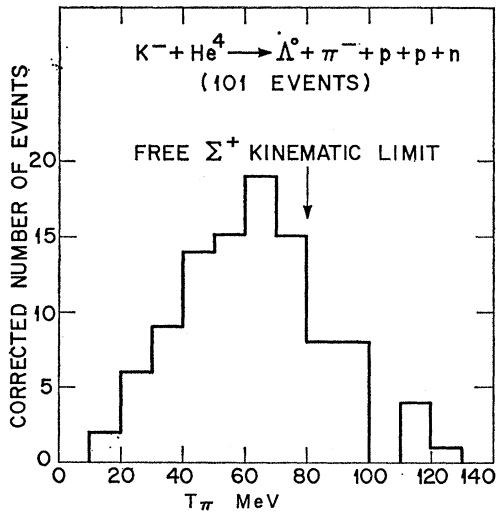

FIG. 24. Pion kinetic-energy distribution for all at-rest $\Lambda\pi^- ppn$ events.

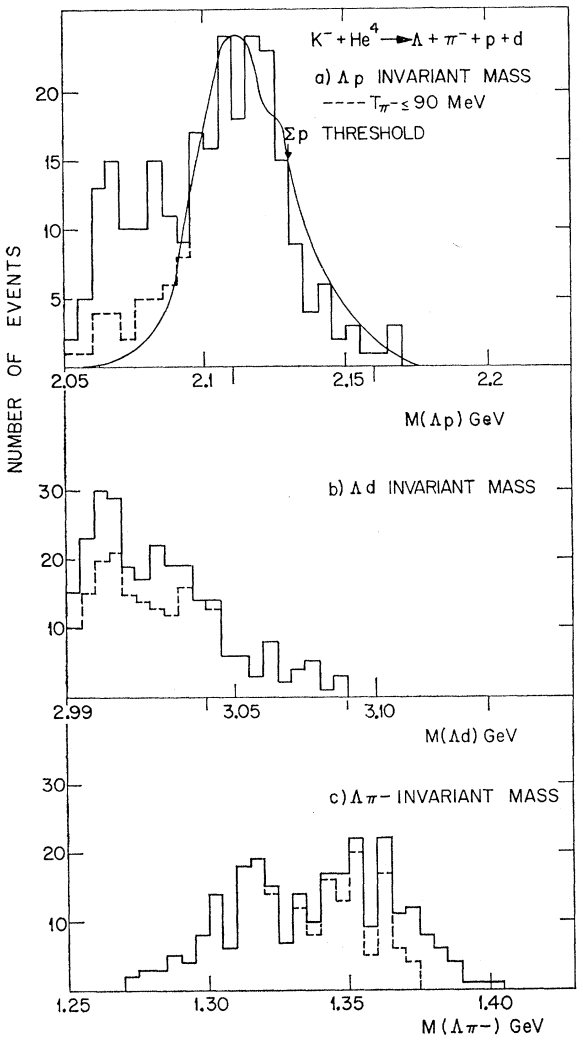

FIG. 25. Invariant mass of (a) Λp, (b) Λd, and (c) $\Lambda\pi$ for at-rest $\Lambda\pi^- pd$ events. The dashed histogram includes events with $T_\pi \leqslant 90$ MeV. The curve in (a) is from the conversion impulse model of Kenyon (Ref. 23) normalized to the events with $T_\pi < 90$ MeV.

by Kotani and Ross[19] for deuterium giving the final state $\Lambda\pi^- p$. Figure 21 gives two sample pion energy distributions as examples.[20] For the reaction $K^-\text{He}^4 \rightarrow \Lambda\pi^- pd$, both of these curves are expected to be only approximate. The curves are only qualitatively in agreement with the experimentally observed distribution, with both curves exhibiting a much sharper peak than observed. It is also evident that the predicted number of events with $T_\pi > 90$ MeV differ substantially in the two theories the model of Sawicki predicting more than the other.

Because of such theoretical uncertainties, an effort was made to isolate the Σ-Λ-conversion-process events experimentally. Transforming into the c.m. system of

[19] T. Kotani and M. Ross, Nuovo Cimento **14**, 1282 (1959).

[20] The sample curve from Sawicki assumes s-state capture and a He^3 form factor of Eichmann as in Ref. 13. The curve of Kotani and Ross is from Ref. 19.

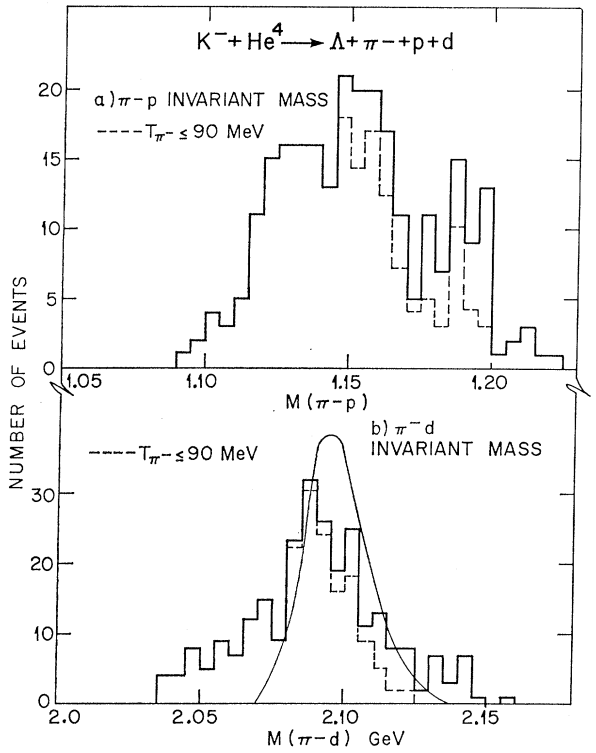

FIG. 26. Invariant mass of (a) $\pi^- p$ and (b) $\pi^- d$ for all at-rest $\Lambda\pi^- pd$ events. The dashed histogram includes events with $T_\pi \leqslant 90$ MeV. The curve in (b) is the "conversion phase space" discussed in the text normalized to number of events with $T_\pi < 90$ MeV.

the baryons, plots were made of the momenta and relative angles of the final-state particles. If Σ-Λ conversion were the dominant process, one would expect the deuteron to act as a spectator while the Λ and proton received the 75-MeV energy from the Σ-Λ mass difference. Hence, the Λ and proton momentum spectra should be peaked at high values, and the angle between the proton and the Λ should tend to 180°.

Figure 22 shows the momentum spectra for the three particles in their over-all c.m. system for two regions of the pion energy. In the region of low pion energy where Σ-Λ-conversion events are expected, it is seen that the proton and Λ have higher momenta than the deuteron. At the higher pion energies, all three particles are seen to have similar spectra. In Fig. 23, the angles between these three particles in the same two regions are shown. All distributions show a backward peaking since the plot is in the three-body c.m. system, but the angle between proton and Λ is far more peaked backwards than the others in the region of low pion energy. For regions of high pion energy, these distributions look very similar. We conclude that for pion energies <90 MeV the spectra qualitatively support a conversion process, while for $T_\pi \geqslant 90$ MeV there is no evidence for conversion. These plots were made for various pion energy cuts, and the maximum difference in the two regions was found for a cut at 90 MeV as shown here. On this basis, it was concluded that (84±4)% of the breakup events $\pi^- \Lambda pd$ originated from the Σ-Λ conversion process, while (15±4)% were from direct Λ production (statistical errors only).

Figure 24 shows the pion kinetic-energy distribution for events fitting the $\pi^- \Lambda ppn$ hypothesis. Again, there is evidence for a peaking at values of the pion energy that are consistent with $\Sigma\pi$ production, indicating the presence of Σ-Λ conversion. The peak is, however, less sharp than for the previous case. Owing to the complexity of the five-body final state and to the loss of events with an invisible proton track, the same analysis as that done for the $\pi^- \Delta pd$ was not carried through. To determine the fraction of conversion and direct process, the 90-MeV pion energy cut was also applied here, giving 84% of the events from Σ-Λ conversion and 16% from direct Λ production. These particular results are only qualitative, since many of the events were not fittable, and this final state very likely reflects complicated double- and triple-scattering effects.

The final state $\Lambda\pi^- pd$ can be used to look for baryon-meson and baryon-hyperon interactions which are not accessible in formation experiments. Figure 25 shows the invariant-mass distributions of the Λp, Λd, and $\Lambda\pi^-$ systems with and without the "direct" Λ events

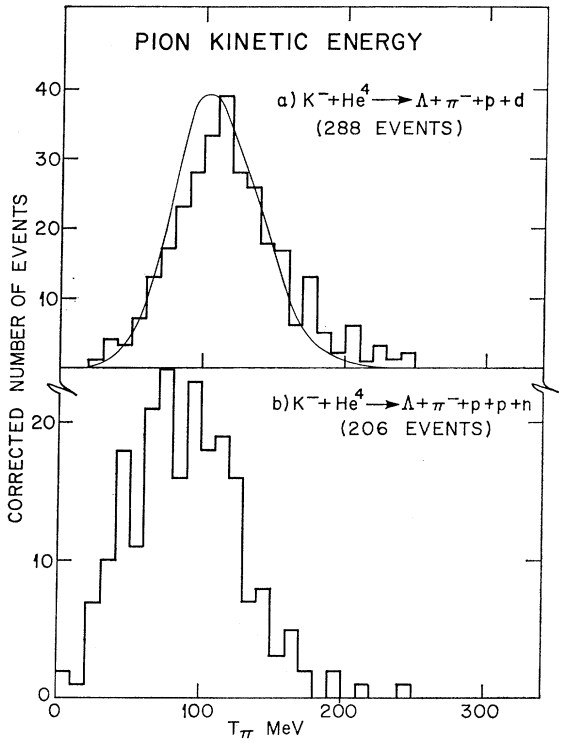

FIG. 27. Pion kinetic-energy distribution in the K^--He^4 c.m. system for all in-flight events ($P_{K^-} \geqslant 125$ MeV/c) fitting (a) $\Lambda\pi^- pd$ and (b) $\Lambda\pi^- ppn$. The curve in (a) shows the impulse prediction for the $\Sigma^0\pi^-$-He^3 final state.

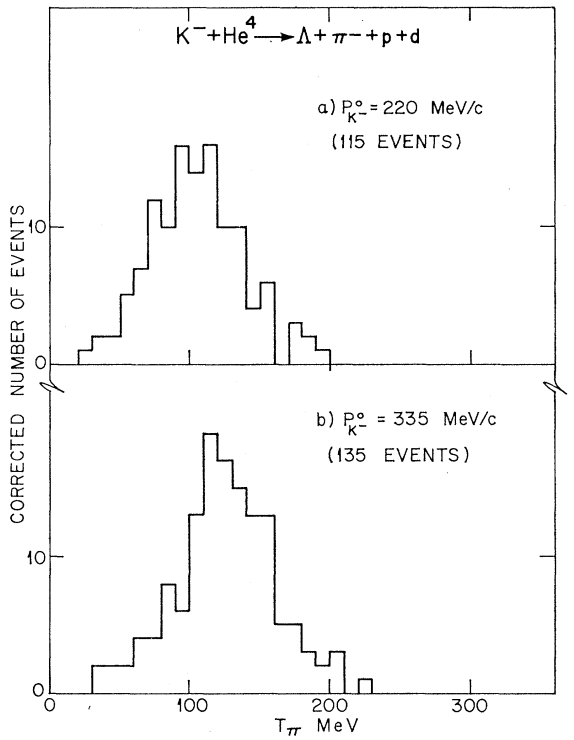

FIG. 28. Pion kinetic-energy distributions in the K^-He^4 c.m. system for in-flight $\Lambda\pi^-pd$ events for two momentum regions: (a) $160<P_{K^-}\leqslant 280$ MeV/c and (b) $280<P_{K^-}\leqslant 370$ MeV/c.

removed. In the Λp final state, Cline *et al.*[21] suggested the possibility of a Λp resonance just below ΣN threshold in the reaction $K^-d\rightarrow\Lambda\pi^-p$ at 400 MeV/c It is unclear on the basis of further experiments[22] whether this enhancement is the result of a Λp resonance or represents a ΣN threshold effect. In the data presented in Fig. 25(a), there is a broad peak in the Λp mass around the ΣN threshold that does seem to originate from Σ-Λ conversion, since the peak is associated with low-energy pions. Also shown in Fig. 25 is a prediction from Kenyon[23] for this final state, assuming that the reaction involves Σ-Λ conversion. The agreement of the model with the data for $T_\pi<90$ MeV is very good.

Neither the Λd nor the $\Lambda\pi$ mass plot shows any evidence for narrow enhancements whether or not the "direct" Λ events are excluded. A possible excited state of the ${}_\Lambda H^3$ hyperfragment might be expected to show an effect on the Λd mass plot. There is a broad peaking at low invariant mass, but this may be an effect of the bound hypernucleus. This plot may be biased at low Λd masses, since the events were required to have a clear Λ vertex. Figure 26 shows the invariant-mass spectrum of the π^-d and the π^-p systems. In the π^-p invariant-mass plot, there is no indication of any structure as expected from the nonexistence of low-mass $T=\frac{1}{2}$ (πN) resonances.

In the π^-d spectrum, there is an apparent enhancement at $M(\pi^-d)\sim 2.08$ GeV. To determine if this peak is a kinematical effect or a resonance, a simple calculation was done based on the hypothesis that the pion originated from the reaction $K^-N\rightarrow\Sigma\pi$ with subsequent Σ-Λ conversion yielding $\Lambda+p$. The neutron was assumed to have its Fermi momentum in the nucleus and the deuteron was considered to be uncorrelated with the pion and emerge as a spectator with its experimentally observed momentum distribution. Using a Monte Carlo program, the π^-d mass distribution was calculated and is shown in Fig. 26. It is apparent that this crude model accounts quite well for the observed peaking in the spectrum so that the peak is very probably a kinematic effect.

The reaction $K^-He^4\rightarrow\Lambda\pi^-pd$ at rest has been studied previously by Kenyon *et al.*[24] The results were compared with an impulse model that treated Σ-Λ conversion by means of a potential well to describe the Σ-nucleus interaction in the intermediate state. The observed distributions were well fitted by using a potential well of depth 37 MeV, without invoking any resonance in the Λp final state.

The data presented here agree with those presented

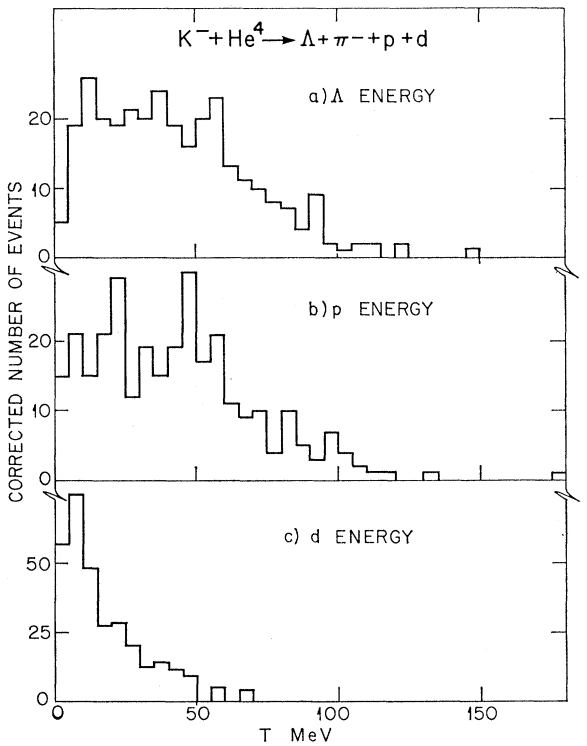

FIG. 29. Kinetic-energy distributions in the K^-He^4 c.m. system for Λ, p, and d for all in-flight $\Lambda\pi^-pd$ events.

[21] D. Cline, R. Laumann, and J. Mapp, Phys. Rev. Letters **20**, 1452 (1968).
[22] T. H. Tan, Phys. Rev. Letters **23**, 395 (1969).
[23] I. R. Kenyon, Nuovo Cimento **55B**, 371 (1968).
[24] I. R. Kenyon, A. E. Sichirollo, C. R. Sun, E. M. Harth, and S. Zenone, Phys. Rev. **165**, 1445 (1968).

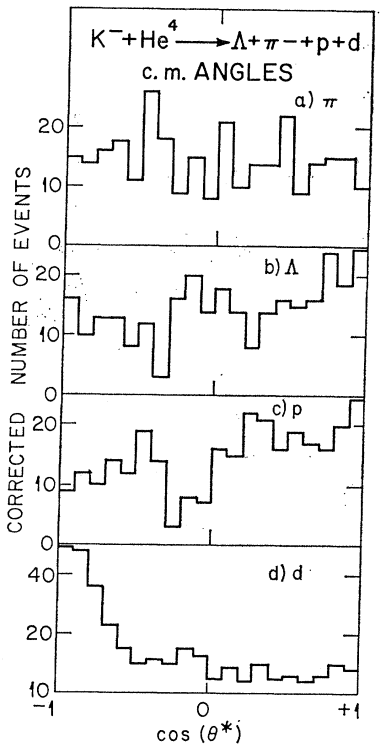

FIG. 30. Center-of-mass angular distributions of Λ, p, and d for in-flight $\Lambda\pi^-pd$ events.

by Kenyon *et al.*,[25] and the conclusion about the strong role played by Σ-Λ conversion is common to both.

D. Reactions $K^-He^4 \rightarrow \Lambda\pi^-pd$ and $K^-He^4 \rightarrow \Lambda\pi^-ppn$ for Kaons in Flight

The pion kinetic-energy spectrum is shown in Fig. 27 for events fitting the $\Lambda\pi^-pd$ and $\Lambda\pi^-ppn$ hypotheses. On the $\Lambda\pi^-pd$ graph, a beam-averaged impulse curve has been shown for the reaction $K^-He \rightarrow \Sigma^0\pi^-He^3$. The similarity of the observed pion spectrum with that of Σ production suggests that these events originate primarily from the Σ-Λ conversion process as was the case at rest. Events involving direct Λ or highly virtual Σ production would have a higher pion energy than for events coming from more real Σ production. There is no evidence for many high-energy pions above the impulse prediction for Σ production. The events fitting $\Lambda\pi^-ppn$ show a spectrum displaced to lower energies compared to the $\Lambda\pi^-pd$ events. For the former reaction, there are many missing events, since the fit is underconstrained when one of the proton tracks is not visible, and thus the spectrum must be used with caution. Nevertheless, the large number of lower-energy pions suggest that Σ-Λ conversion is involved. This is the same kind of behavior observed in the at-rest sample for the same final state. Figure 28 shows the pion energy plot for $\Lambda\pi^-pd$ events in the two beam-momentum regions for comparison with the bound He^3 spectrum shown in Fig. 16.

Since the $\Lambda\pi^-pd$ events represent a complete sample with the exception of rare cases where both the proton and deuteron are invisible, these can be used for final-state interaction studies. Figure 29 shows the energy distributions for the other particles. The similarity of the Λ and proton spectra is obvious, while the deuteron has a distribution shited to lower energies. This suggests that the deuteron again acts as a spectator while the Λ and proton are participating in the conversion interaction $\Sigma N \rightarrow \Lambda p$. Figure 30 shows the angular distribution for each of the final particles as measured in the over-all c.m. frame with respect to the incident kaon direction. The deuteron differs from the others in that it peaks sharply backwards which is further evidence for its spectator nature.

Figure 31(a) shows the invariant mass of the $\Lambda\pi^-$ system from the events fitting $\Lambda\pi^-pd$. There is seen to be a peaking in the region of 1380 MeV that might correspond to the production of the $Y_1^*(1385)$ resonance. Figure 32 shows a similar plot of the $\Lambda\pi^-$ invariant mass for the $\Lambda\pi^-pd$ events in two different regions of beam momentum. The general position of the peak is seen not to change very much.

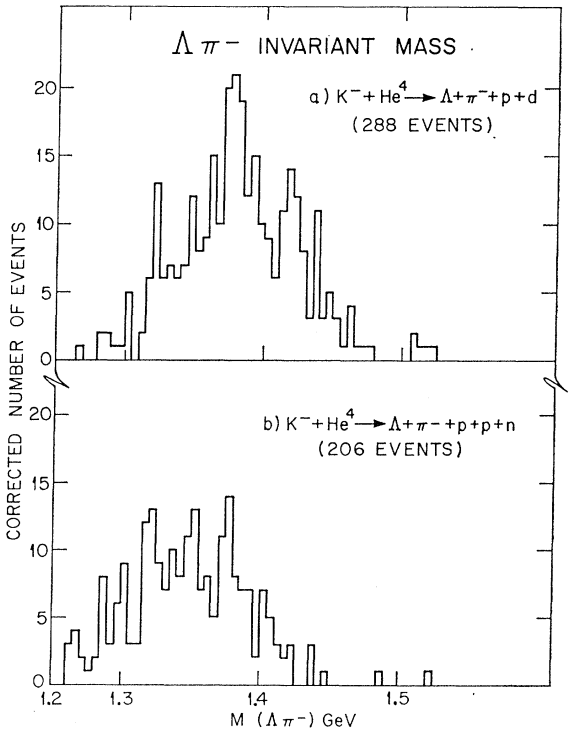

FIG. 31. $\Lambda\pi^-$ invariant-mass distributions for all in-flight events fitting (a) $\Lambda\pi^-pd$ and (b) $\Lambda\pi^-ppn$.

[25] The ratio of $\pi^-\Lambda ppn$ to $\pi^-\Lambda pd$ events found in Kenyon's results was somewhat higher than that observed in the present experiment. This is possibly due to ambiguous events, which in the present analysis were all assigned to the $\Lambda\pi^-pd$ hypothesis.

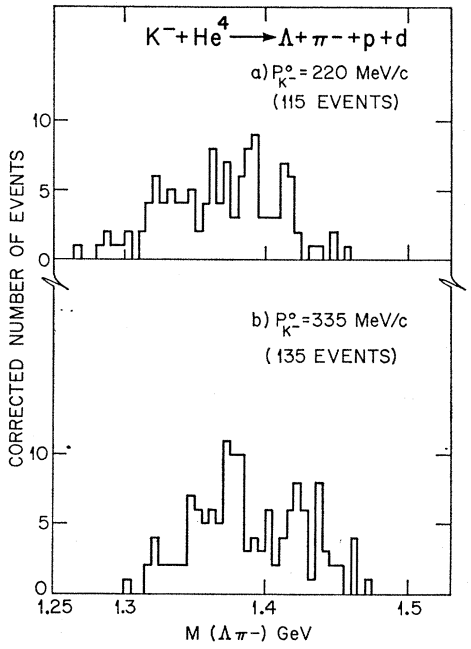

FIG. 32. $\Lambda\pi^-$ invariant-mass distribution for $\Lambda\pi^- pd$ events in the two beam-momentum regions.

Since this final state seems to be originating in large part from Σ-Λ conversion, it is possible that this peak in the $\Lambda\pi^-$ spectrum could come from that process. In the $K^- d \rightarrow \Lambda\pi^- p$ reaction at 400 MeV/c studied by the Wisconsin group,[26] the conversion events were easily identifiable. They observed, however, a uniform distribution in the $\Lambda\pi^-$ invariant mass from the Σ-conversion events. There was a peak in the $\Lambda\pi^-$ spectrum (at 1440 MeV), but it probably originated from a secondary beam scattering. Such scattering processes are cetainly occurring in the present experiment, but the theoretical calculation is far more complex than that for deuterium. It appears, however, on the basis of the Wisconsin results, that the peak at 1380 MeV is not likely to be a kinematic effect of Σ comversion.

If a Y_1^* is produced in this breakup reaction, then the reaction mechanism is probably not impulsive since impulsive reactions usually lead to a bound He^3. One possible origin of this resonance is the reaction $K^- 2N \rightarrow Y_1^* p$, which is equivalent to a double-scattering effect different from that mentioned above. The kinematics of such a process are similar to the Σ-Λ-conversion reaction. Both processes lead to a relatively fast proton as observed in Fig. 29, and both leave the deuteron as a spectator. In addition, both processes would yield a pion energy spectrum consistent with that experimentally observed.

The laboratory angular distribution of the deuteron deviates only slightly from isotropy, consistent with the behavior of a spectator. Both the proton momentum and the kaon-deuteron laboratory angle were examined in different regions of the $\Lambda\pi^-$ invariant mass to look for different behavior in the immediate region of the enhancement as compared to regions far from the peak. No noticeable variation was observed in the different regions.

The processes of Σ-Λ conversion and Y_1^* production are not mutually exclusive, and the Y_1^* enhancement could well originate from a $\Lambda\pi^-$ final-state interaction following Σ-Λ conversion. Thus, the exact origin of this peak remains unclear. In the at-rest case, the $\Lambda\pi^-$ invariant-mass distribution showed no similar enhancement [see Fig. 25(c)].

There are other possible final-state effects of interest. Figure 33(a) shows the invariant mass of the $\pi^- p$ system. There is no evidence for structure, consistent with expectations for an $I = \frac{1}{2}$ state. Figure 33(b) shows the invariant-mass distribution of the $\pi^- d$ system compared to the predictions of the Monte Carlo calculation discussed for the same final state produced by kaons at rest (Fig. 26). Again, there is a substantial similarity between the curve and the data. Since the model actually describes a sort of "conversion phase space" for the $\pi^- d$ invariant mass, it would appear that there is nothing in the data to suggest a πd resonance. The D^* that is often seen in πd final states at 2175 MeV does not seem to be evident here. This peak, related to

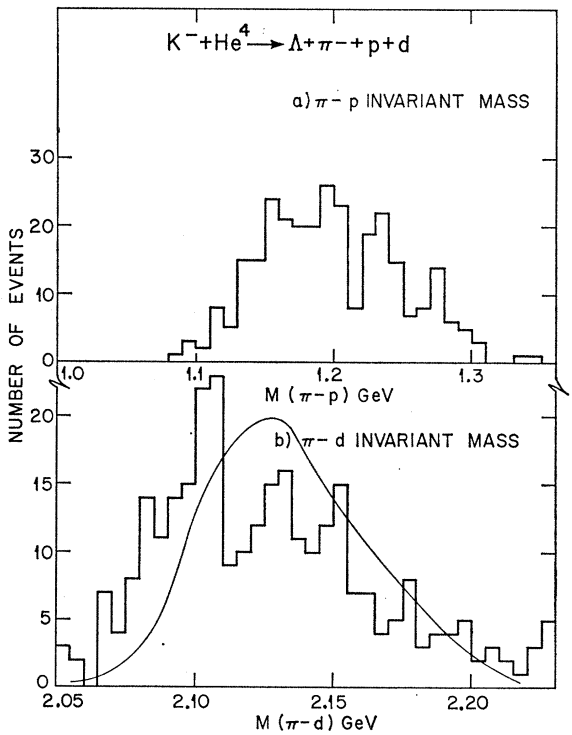

FIG. 33. (a) $\pi^- p$ and (b) $\pi^- d$ invariant mass distribution for all in-flight $\Lambda\pi^- pd$ events. The curve in (b) is the "conversion phase space" discussed in the text, normalized to the total number of events.

[26] R. Laumann (private communication).

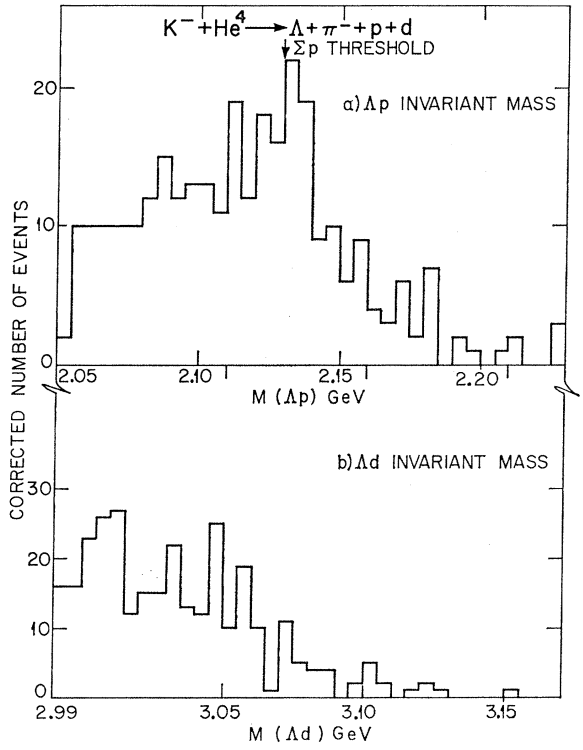

FIG. 34. (a) Λp and (b) Λd invariant-mass distributions for all in-flight $\Lambda\pi^- pd$ events.

$N^*(1236)$ formation in the nucleus, would give a very board enhancement.

The invariant-mass distributions of the Λp and Λd systems are shown in Fig. 34. In both cases, the spectrum is very similar to that observed in the at-rest events (Fig. 25) with no sign of structure. For the Λp events, it was not possible to remove the examples of "direct" Λ production since they were not identifiable. The appearance of a large number of events at low value of Λp mass (<2.1 GeV) shows that not all of the events originate from conversion. Although there is no impulse-model prediction to compare with in this case, the general agreement of the distributions shown in Figs. 25(a) and 34(a) suggests that the broad peak at 2130 MeV observed for in-flight kaons is a result of a $\Sigma N \rightarrow \Lambda N$ process.

There have been several recent models that predict a Λp resonance very close to the ΣN threshold.[27,28] The work presented by Downs,[29] using a boson-exchange potential, predicts a ΛN resonance so close to threshold that an experimental resolution of a resonance as distinct from a threshold cusp phenomenon is very difficult. The data presented here are certainly inadequate to determine if the broad peak observed results from a threshold effect or a resonance or both.

[27] J. C. Helder and J. J. de Swart, in Ref. 11, p. 852.
[28] G. Fast and J. J. de Swart, in Ref. 11, p. 814.
[29] B. W. Downs, in Ref. 11, p. 51.

IV. REACTION BRANCHING RATIOS AND CROSS SECTIONS

A separate scan was made to determine the number of stopping-K^- tracks for the at-rest film. This was done by scanning 18 of the 41 rolls every twentieth frame for all K^- interactions. The in-flight interactions were removed by using the momentum of the measured beam tracks. The final result was 0.24 ± 0.02 stopping K^- per frame.

The branching ratios obtained for the various reactions from K^- at rest are shown in Table VI. The numbers include an estimate[30] of the number of events missed when the hypothesis was underconstrained as well as the usual corrections for Λ neutral decay, etc. The numbers are in reasonable agreement with those obtained in a comprehensive analysis of a small sample of stopping K^- in helium.[31]

The cross sections for the various final states were calculated as a function of beam momentum using data from the in-flight film. The beam flux was deduced by scanning five of the 20 rolls for τ decays. The cross sections were calculated for the same two regions of beam momenta as those used in the figures. The results are given in Table VII.

Table VIII compares the predicted cross sections in the two momentum regions with the experimental measurements for the final states $\Lambda\pi^-\mathrm{He}^3$ and $\Sigma^0\pi^-\mathrm{He}^3$. The two theoretical predictions were calculated from the impulse model and used, first, the pure Kim amplitudes and, second, the $SU(3)$ amplitude for P_{13} setting P_{11} equal to zero. The fact that both of the theoretical cross sections are within a factor of 2 of the experimental results must be regarded as rather remarkable in view of the simplicity of the model. In view of the various approximations in the theory, it does not seem possible to draw any definitive conclusions favoring the Kim or the $SU(3)$ amplitudes.

V. Σ^0-Λ CONVERSION

For the at-rest events, the impulse model predicts the relative rates of $\Lambda\pi^-\mathrm{He}^3$ and $\Sigma^0\pi^-\mathrm{He}^3$ production. By comparing these rates with experiment, the fraction

TABLE VI. (Branching ratios)/(stopping K^-).

Final state	Branching ratio
$\pi^-\,\Lambda\,\mathrm{He}^3$	$0.092_{-0.005}^{+0.009}$
$\pi^-\,\Sigma^0\,\mathrm{He}^3$	$0.01_{-0.0005}^{+0.0018}$
$\pi^-\,\Lambda\,pd$	$0.072_{-0.003}^{+0.005}$
$\pi^-\,\Lambda\,ppn$	$0.063_{-0.003}^{+0.006}$

[30] This estimate was obtained by considering the number of events that had a connecting Λ but no production fit. These were assigned to the respective hypotheses based on the relative probability that the hypothesis would be constrained, as determined from the fitted spectra.
[31] P. A. Katz, K. Bunnell, M. Derrick, T. Fields, L. G. Hyman, and G. Keyes, Phys. Rev. D 1, 1267 (1970).

TABLE VII. Experimental cross sections.

Hypothesis \ Momentum range (MeV/c)	$160 \leqslant P_{K^-} \leqslant 280$ Cross section (mb)	$280 \leqslant P_{K^-} \leqslant 370$ Cross section (mb)
$\pi^- \Lambda$ He^3	17.0±4.1	8.6±1.6
$\pi^- \Sigma^0$ He^3	3.0±1.1	2.8±0.7
$\pi^- \Lambda$ pd	17.5±4.2	8.0±1.6
$\pi^- \Lambda$ ppn	15.8±5.1	8.1±2.0
$\pi^- \Sigma^0$ pd	1.0±0.5	0.6±0.3
$\pi^- \pi^+ \Lambda$ (ppn)	0.0	0.2±0.1

of Σ^0 converting internally to yield a Λ can be estimated. The Σ^0/Λ ratio at production is predicted to be 0.49 using Kim's amplitude and 0.45 for the $SU(3)$ case. Experimentally, the ratio is measured to be 0.14±0.02, which indicates that the fraction of produced Σ^0 that convert to Λ is (70±4)%, in agreement with previous estimates.[31]

The cross sections given in Table VIII show an experimental depletion of Σ^0 events and an excess of Λ events over the predictions of the impulse model. The $SU(3)$ prediction for the $\Sigma^0\pi^-He^3$ cross section is not very much different from the Kim prediction for the channel because of weak coupling of Y_1^* to $\Sigma\pi$. Assuming that the loss of events is due to Σ conversion, and using the $SU(3)$ cross sections, the results are that (62±15)% of the Σ hyperons produced by the lower-momentum kaons convert and (41±15)% at the higher beam momentum. A decrease in the $\Sigma N \to \Lambda N$ cross section as the beam momentum is increased is also observed in Σ interactions in hydrogen.[32]

VI. SEARCH FOR POSSIBLE Λn BOUND STATE

Using the events with two positive prongs, a search was undertaken for a possible Λn bound state. This was done by looking at three-prong V^0 events with a stopping K^- that either did not give a Λ decay fit or in which the fitted Λ did not connect with the production vertex. The expected reaction would be $K^-He^4 \to \pi^- pp(\Lambda n)$, with the bound state (Λn) having a mass close to Λn threshold. To search for this, the missing mass from the $\pi^- pp$ system was calculated using kinematical quantities from the geometry program and is

TABLE VIII. Cross-section comparisons.

Hypothesis	Momentum region (MeV/c)	σ_{expt} (mb)	σ_{Kim} (mb)	$\sigma_{SU(3)}$ (mb)
$\pi^- \Lambda$ He^3	$160 \leqslant P_{K^-} \leqslant 280$	17.0±4.1	9.2	14.1
$\pi^- \Lambda$ He^3	$280 < P_{K^-} \leqslant 370$	8.6±1.6	4.6	8.0
$\pi^- \Sigma^0$ He^3	$160 \leqslant P_{K^-} \leqslant 280$	3.0±1.1	6.8	7.8
$\pi^- \Sigma^0$ He^3	$280 < P_{K^-} \leqslant 370$	2.8±0.7	3.9	4.7

[32] R. Engelmann, H. Filthuth, V. Hepp, and E. Kluge, Phys. Letters 21, 587 (1966).

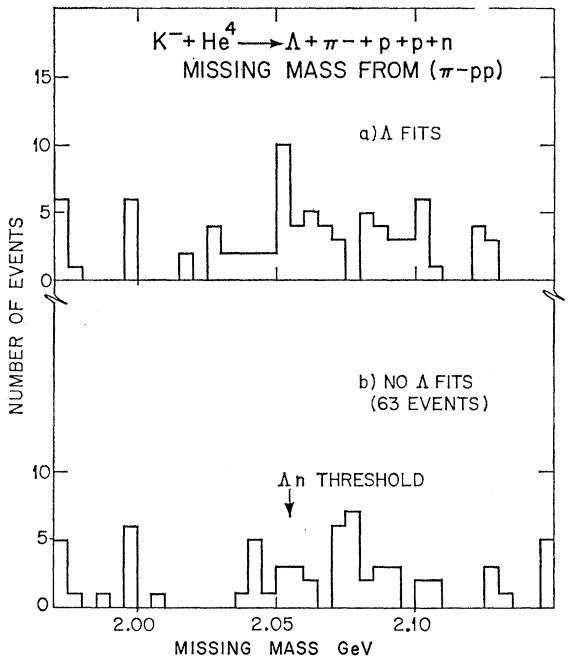

FIG. 35. Missing mass of X for three-prong V^0 events in the final-state $\pi^- ppX$ as determined from geometry program parameters: (a) events giving a Λ production fit; (b) events either having a nonconnecting Λ or no Λ fit at all.

shown in Fig. 35. The events appearing below Λn threshold in Fig. 35 came from the final-state $\Lambda\pi^- pd$ where the deuteron was assumed (in this calculation) to be a proton. There is no evidence for an excess of events at Λn threshold for the nonfitting or nonconnecting Λ events as compared with the control sample which was provided by the events giving Λ fits. Events of the final state $\pi^-\Lambda ppn$ will often give a Λn mass close to threshold, and it is likely that most of the time (~80%) such events could not be kinematically distinguished from events that included a Λn bound state decaying to $\pi^- pn$.[33]

Consequently, an attempt was made to fit the nonfitting and nonconnecting Λ events to the hypothesis $K^-He^4 \to \pi^- pp(\Lambda n)$, where the Λn was taken at threshold mass and considered to be a missing neutral in the fit. There were 13 events that gave a one-constraint fit to this hypothesis. The space angles found for the (Λn) system were compared to the production angles observed for the V^0. In no case did the observed V^0 vertex lie within 3 standard deviations of the direction found for the missing Λn system. All events with a nonfitting or nonconnecting Λ were also tried to the hypothesis

$$K^-He^4 \to \pi^- ppn(\Lambda n)$$
$$\searrow$$
$$\pi^- d,$$

[33] This follows from the analysis of the ${}_\Lambda H^3$ hyperfragment which shows that most of the three-body decays of ${}_\Lambda H^3$ also fit the free-Λ hypothesis; see Ref. 1.

which, if found, would be an unambiguous event. No event fitted this hypothesis.

The lack of any candidates leads to the conclusion that the production rate for a Λn bound state from K^- absorption at rest in helium is $\leqslant 5\times10^{-4}$ per stopping K^- at 70% confidence. This rate allows for the possibility of the 80% overlap with $\Lambda\pi^- ppn$ fits as mentioned above.

Two recent experiments have also measured an upper limit for the production of a $(\Sigma^- n)$ bound state. One experiment,[34] using stopping K^- in helium, deduced that the production rate for a $(\Sigma^- n)$ bound state was $\leqslant 2\times10^{-4}$ per stopping K^-, which is similar to the limit arrived at here for the (Λn) bound state. Another experiment,[35] using a K^- deuterium exposure at 400 MeV/c, found the upper limit on the cross section for a $(\Sigma^- n)$ bound state to be 15 μb.

VII. SUMMARY

Both of the previous experimental determinations[8,36] of the $\bar{K}NY_1^*$ coupling involved the analysis of physical-region data and an extrapolation below the $\bar{K}N$ threshold to the region of the $Y_1^*(1385)$. In the present analysis, an attempt to investigate the $\bar{K}NY_1^*$ coupling strength was carried out by utilizing a virtual neutron in the helium nucleus to observe the reaction $\bar{K}N \rightarrow Y_1^*(1385)$ directly at the resonant energy.[37] In this application of the impulse model, the question of the helium form factor, the orbital-atomic-capture state, and final-state interactions complicated the analysis.

For the He^3 kinetic-energy spectrum, the use of the value predicted by $SU(3)$ for the P_{13} wave improved the fit over that obtained with Kim's values for the P-wave matrix elements. The best fit to the data for $\Lambda\pi^-He^3$ produced by K^- at rest was found with a Hulthén form factor, an $SU(3)$ P_{13} amplitude, and a mixture of 70% s-wave and 30% p-wave atomic-capture states. The possible presence of residual Σ-Λ conversion and other final-state effects are factors whose influence on these conclusions is difficult to evaluate.

The Σ-Λ conversion process was seen to play a major role in Λ production, accounting for most of the events where the He^3 nucleus broke up. The fraction of Σ^0 converting was determined and was observed to decrease with increased c.m. energy. In the interaction of kaons at rest, it was found that (14 ± 3)% of all conversion events left a bound He^3, although this fraction was smaller for in-flight interaction.

For the $\Lambda\pi^-He^3$ final state produced by kaons in flight, there were insufficient data to resolve the small differences in form factors or $\bar{K}N$ matrix elements. There was no evidence from the in-flight data for a $\Lambda\pi^-$ enhancement at 1440 MeV as observed by Cline *et al.*, suggesting that the peak is the result of a second-scattering effect. In the $\Lambda\pi^- pd$ final state, there was no specific evidence for a narrow resonance in the Λp system near the ΣN threshold.

A search for a Λn bound state found no candidates and an upper limit for its production was placed at 5×10^{-4}/(stopping K^-).

ACKNOWLEDGMENTS

We wish to thank the ZGS Operations Group and the bubble-chamber technicians for their essential aid in obtaining the pictures. The film was efficiently scanned and well measured by Hope Chaffee, Modesta Umbrasas, Chris Dedin, and Joyce Brandolino. Jim Loken and Tom Wangler gave considerable help in the early stages of the analysis of this experiment. Phil Katz and Tom Kotek contributed effort with the computing.

[34] R. A. Burnstein, W. C. Cummings, D. L. Swanson, and V. R. Veirs, Phys. Rev. **177**, 1945 (1969).
[35] D. Cline, R. Laumann, and J. Mapp, in Ref. 11, p. 92.
[36] R. D. Tripp, R. O. Bangerter, A. Barbaro-Galtieri, and T. S. Mast, Phys. Rev. Letters **21**, 1721 (1968).
[37] See also K. Bunnell, D. Cline, R. Laumann, J. Mapp, and J. Uretsky, Nuovo Cimento Letters **3**, 224 (1970).